ANALYTICAL DESCRIPTION OF OPTICAL GYROS

Paul G. Savage
Strapdown Associates, Inc.
Maple Plain, MN 55359 USA

WBN-14024
www.strapdowassociates.com
April 3, 2019 (Updated November 6, 2022 and March 15, 2024)

ABSTRACT

Ring laser gyros (RLGs) and fiber optic gyros (FOGs) measure angular rotation by the phase difference generated between oppositely directed monochromatic light waves traversing a closed optical waveguide embedded in the gyro structure. This article presents a comprehensive analytical development showing how the rotation induced phase difference is created at the gyro readout photo detector by two effects, 1} A wavelength difference between the oppositely directed waves caused by classical Newtonian/Euclidean geometrical effects (the same predicted by Special Relativity when rotation induced velocity of the waveguide is small compared to the speed of light), and 2} The speed of light being the same relative to the rotating gyro as it is in non-rotating inertial space, an exclusive result of Relativity. This contrasts with previous explanations attributing rotation induced phase shift to a difference in optical path length between the oppositely directed waves, or to a time difference for the oppositely directed waves to traverse the waveguide. These explanations, however, were with respect to non-rotating space, not to the rotating gyro readout used for angular rotation measurements. Relative to the readout (as in this development), it is shown that the time for each of the oppositely directed waves to traverse the waveguide is the same. This article first derives a general equation describing how rotation induces a change in optical power when the oppositely directed beams are combined to illuminate the readout detector. Applying the equation to an RLG shows how cyclic outputs are generated from the photo detector, each representing a known increment of angular rotation. Application to a FOG shows how successive angular rotation increments are measured, each over the time for the waves to traverse the fiber coil. Analysis of "closed-loop" FOG operations shows how to operate lithium–niobate crystals inserted in the fiber coil to balance rotation induced phase shift while generating angular rotation outputs.

FOREWORD

This article is a second revised version of its second publication [1], modified here for expanded and clarified derivations translating wavelength results into their impact on optical light wave interactions at the gyro pickoff. Results and conclusions are unchanged from [1].

INTRODUCTION

Optical gyros (ring laser and fiber optic) have been in broad usage since the late 1970s. Curiously, however, their basic principle of operation has varied between designers and users. Optical gyros measure the change in phase induced by angular rotation in oppositely directed monochromatic light waves created within the gyro. Some attribute the phase change to Relativity theory while others characterize it as a classical kinematic Doppler effect. Many of these and other explanations have relied on heuristic reasoning to explain actual measured optical gyro operating characteristics. The purpose of this article is to provide a rigorous comprehensive analytical derivation of equations governing the operation of optical gyros and in the process, identify those attributed to classical vector kinematics, and those uniquely contributed by Relativity. The analysis is based on idealized optical gyro configurations in which oppositely directed light waves occupying the same physical space are independent from one-another, unaffected by imperfections in the closed waveguide directing their motion within the gyro, and having the same polarization direction when combined at the readout photo detector.

Relativity theory relates the motion of a point in space as measured by two remote observers in motion relative to one-another. When the velocity magnitude between observers is small compared to the speed of light, the observed motion forecasted by Special Relativity theory [2 Part 1; 3 Chpt VI; 4] reduces to classical Newtonian/Galilean kinematic predictions [2 pp 37-38; 3 Chpt III Sect 7; 5 Sect 12-1]. Such is the case for optical gyros when analyzing how angular rotation impacts each of two oppositely directed light waves travelling within the gyro along a common closed optical path. Similar to the Doppler-like frequency shift observed in light waves emanating from receding stars, both Galilean and Relativistic kinematics predict an angular rotation induced wavelength shift in the optical gyro light waves, increasing for the wave travelling in the direction of rotation, decreasing for the oppositely directed wave. Coupled with the wavelength shift, Relativity predicts that the propagation speed for each of the oppositely directed light waves will be the same "speed-of-light" relative to the rotating waveguide, the same as for light waves propagating through non-rotating inertial space. Light wave frequencies equate to the speed-of-light constant divided by their wavelength, thus, decrease for waves travelling with rotation and conversely for oppositely directed waves, generating a frequency difference between the oppositely directed waves. When the oppositely directed waves are mixed by the gyro readout, a combined beam power signal is generated whose intensity measures the rotation induced frequency difference. The combined beam power illuminates a readout photo detector, thereby generating a measurement of angular rotation. This is exactly what is produced in operating optical gyros under rotation, and what is predicted by the analytical development in this article.

Beginning from classical vector geometry, this article first analytically describes the distance vector to the same remote point in space as measured by each of two observers. Classical Newtonian kinematics then describes how the observed remote point location is impacted by relative motion between the observers. The equivalent result is also derived in Appendix A based on Special Relativity theory, producing the same Galilean/Newtonian derived result when the relative velocity magnitude between observers is small compared to the speed of light.

Both the Galilean/Newtonian and Relativity results are derived in non-rotating coordinates. The article then derives the equivalent in rotating coordinates by projecting the relative position vector geometry onto two non-rotating coordinate frames, one rotated from the other by a small angular rotation. The difference between the two projections is identified as the change that would be measured in a rotating coordinate frame undergoing the small angular rotation. Substituting the original non-rotating coordinate result, derives an equation relating the motion of the remote point as measured by one observer in non-rotating coordinates, in terms of the differential measurement taken by the other observer in rotating coordinates.

The analytical development to this point in the article is general in nature. Continued analysis specializes the two observation points to be fixed within a rigid body (a gyro), defining the observed point in motion to be a photon of light traversing a waveguide within the gyro, defining one of the observation points to be within the waveguide at the start of a photon's motion, the other observation point at a reference "rotation center" external to the waveguide, with gyro rotation equated to that of the rotating coordinate frame. In the process, the photon in motion is defined to be part of a travelling light wave whose wavelength relative to the rotating gyro is a function of the wavelength in non-rotating space, the distance from the reference point to the photon, and the gyro's angular rotation during the time the photon traverses a wavelength of distance. The wavelength solution is then used to obtain independent integral solutions for each of the oppositely directed light waves traversing the gyro waveguide.

Combining the individual light wave solutions in the readout zone at the same instant of time (a common intersection in space/time) requires application of Relativity theory. The method is to first recognize that in a non-rotating frame, the wave propagation speed at any point in the waveguide will be at the same speed-of-light constant as it is open-space. Second, for the observer stationed in the rotating waveguide, the small movement of a passing photon, although rotated through a small amount, will (to first order in the rotation angle) be of the same magnitude as when measured in a non-rotating frame at the same location. By joining these observations, it is analytically shown that relative to the rotating waveguide, the propagation rate for each of the oppositely directed beams will be at the same speed-of-light, hence, the time interval for each wave to traverse a given distance relative to the waveguide will also be the same. Applying this finding to each of the oppositely directed waves allows them to be analytically summed (at a common space/time location) into a single equation defining the beam power that will illuminate the gyro readout photo detector(s). The result equates the cumulative difference in phase between the individual waves to the integrated effect of angular rotation over a selected time interval. For the remainder of the article, the combined beam power equation is used to explain the operating characteristics of fiber optic and ring laser optical gyros.

Two types of ring laser gyro configurations are described, those in which the closed waveguide is constrained by reflecting mirror geometry to lie within a plane, and those in which the mirrors are angularly oriented to create a closed out-of-plane waveguide geometry. The results for each analytically demonstrates how combining the oppositely directed waves at the gyro readout creates an optical interference pattern that moves across the photo detector(s) at a linear rate proportional to the gyro angular rate thus generating cyclic outputs, each representing a known increment of angular rotation.

The combined beam power equation is then used to analytically describe two types of fiber optic gyros, those classified as "open-loop" and those classified as "closed-loop". By injecting phase bias into the light waves with lithium-niobate (L/N) integrated-optics crystals inserted in the fiber coil, the closed-loop configuration provides control bias to the oppositely directed light beams that adds to the phase induced by angular rotation. Using outputs from the gyro photo detector, L/N bias command equations are derived to balance the rotation induced phase, while simultaneously generating successive outputs of gyro angular rotation over the time for a light wave to traverse the fiber coil. Included in the L/N bias equations are provisions to eliminate round-off error generated by three closed-loop electronics interface operations; 1) Digitally sampling photo detector analog measurements into the digital control loop processor, 2) Creating L/N analog bias control voltages from the digital control-loop processor, and 3) Converting angular rotation increments calculated in the control-loop processor for digital output format compatibility.

FOG configurations can generally be categorized as of the interferometric or resonant type (IFOGs or RFOGs). In all FOGs, radiation from an external light source is gated into a fiber optic coil to form overlapping oppositely directed light waves that span a fiber optical coil for eventual output sampling. In an IFOG, the radiation traverses the fiber optical coil once. To compensate for imperfections in their construction, resonant RFOG configurations have evolved in which the externally input light beam is recirculated several times before output sampling. All FOG configurations described in this article are exclusively of the idealized (error free) interferometric type (IFOGs).

NOTATION

The following general notation is used in the article:

$\underline{V}$ = Vector parameter having length and direction. Vectors in this article are classified as "free vectors" having no preferred location in coordinate frames in which they are analytically described.

$/\, i$ = Subscript denoting the vector parameter being observed (measured or calculated from measurements) at observation point i (i being point a or b).

Observable Event = An event at a position location in space at a particular instant of time (e.g., a lightning strike, explosion, illumination by a radar pulse, or passage of the leading edge of a light wave across a point in space) that can be observed at a remote spatial location based on electro-magnetic wave propagation (e.g. light or radar) [2 pp 29, 36; 3 pp 28, 236-238; 6 pp 10].

$k : t$ = A particular location in space/time at spatial point k at time t.

DIFFERENTIAL POSITION MOTION IN NON-ROTATING COORDINATES

In non-rotating coordinates, Fig. 1 illustrates the geometrical relationship between distance vectors from two observation points *a* and *i* to a remote point *p* at the same instant of time.

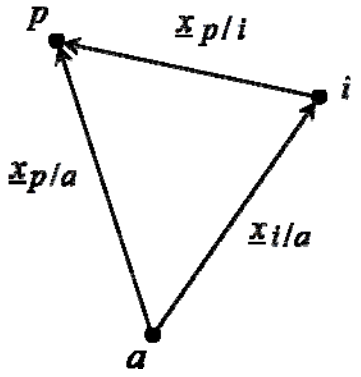

Fig. 1 – Position Vector Relationships At The Same Instant Of Time
In Non-Rotating Coordinates

In Fig. 1, $\underline{x}_{p/a}$ is the distance vector to point *p* determined (observed) from point *a*, $\underline{x}_{p/i}$ is the distance vector to point *p* observed from point *i*, and $\underline{x}_{i/a}$ is the distance vector to point *i* determined at point *a*. At two successive time points t_1 and t_2 (t_2 following t_1), the kinematic representation in Fig. 1 can be described analytically by

$$\underline{x}_{p_1/a} = \underline{x}_{p_1/i} + \underline{x}_{i_1/a} \qquad \underline{x}_{p_2/a} = \underline{x}_{p_2/i} + \underline{x}_{i_2/a} \tag{1}$$

where subscripts 1 and 2 identify point locations at t_1 and t_2. The changes in the Fig. 1 vector parameters between the t_1 and t_2 time instants are defined as

$$\Delta\underline{x}_{p/a} \equiv \underline{x}_{p_2/a} - \underline{x}_{p_1/a} \qquad \Delta\underline{x}_{p/i} \equiv \underline{x}_{p_2/i} - \underline{x}_{p_1/i} \qquad \Delta\underline{x}_{i/a} \equiv \underline{x}_{i_2/a} - \underline{x}_{i_1/a} \tag{2}$$

Taking the difference between the (1) equations and applying the (2) definitions finds

$$\Delta\underline{x}_{p/a} = \Delta\underline{x}_{p/i} + \Delta\underline{x}_{i/a} \tag{3}$$

IDENTIFYING COORDINATE FRAMES

Eqs. (1) – (3) are valid in any non-rotating coordinate frame. As in [7], let us now introduce non-rotating coordinate frames B_1 and B_2 defined as parallel to the instantaneous orientation of rotating coordinate frame *B* at successive time instants t_1 and t_2. Because B_1 and B_2 are non-rotating relative to a common non-rotating space, the angular orientation of B_2 relative to B_1 will

be constant. For clarity, the $\Delta\underline{x}_{p/i}$ and $\Delta\underline{x}_{i/a}$ definitions in (2) are now rewritten in B_1 coordinates as

$$\Delta\underline{x}^{B1}_{p/i} = \underline{x}^{B1}_{p_2/i} - \underline{x}^{B1}_{p_1/i} \qquad \Delta\underline{x}^{B1}_{i/a} = \underline{x}^{B1}_{i\,2/a} - \underline{x}^{B1}_{i1/a} \tag{4}$$

where the B_1 superscripts identify the B_1 non-rotating coordinate frame in which the vector components are projected (e.g., as elements of a column matrix). The constituents of $\Delta\underline{x}^{B1}_{p/i}$ and $\Delta\underline{x}^{B1}_{i/a}$ in (4) can now be related to distance vector measurements taken in B_2 non-rotating coordinates coupled with the angular orientation relating the B_1 and B_2 coordinate frames:

$$\begin{aligned}
\Delta\underline{x}^{B1}_{p/i} &= \underline{x}^{B1}_{p_2/i} - \underline{x}^{B1}_{p_1/i} = C^{B1}_{B2}\,\underline{x}^{B2}_{p_2/i} - \underline{x}^{B1}_{p_1/i} = \left(C^{B1}_{B2} - I + I\right)\underline{x}^{B2}_{p_2/i} - \underline{x}^{B1}_{p_1/i} \\
&= \underline{x}^{B2}_{p_2/i} - \underline{x}^{B1}_{p_1/i} + \left(C^{B1}_{B2} - I\right)\underline{x}^{B2}_{p_2/i} \\
\Delta\underline{x}^{B1}_{i/a} &= \underline{x}^{B1}_{i\,2/a} - \underline{x}^{B1}_{i1/a} = C^{B1}_{B2}\,\underline{x}^{B2}_{i\,2/a} - \underline{x}^{B1}_{i1/a} = \left(C^{B1}_{B2} - I + I\right)\underline{x}^{B2}_{i\,2/a} - \underline{x}^{B1}_{i1/a} \\
&= \underline{x}^{B2}_{i\,2/a} - \underline{x}^{B1}_{i1/a} + \left(C^{B1}_{B2} - I\right)\underline{x}^{B2}_{i\,2/a}
\end{aligned} \tag{5}$$

where superscript B_2 identifies vector component projections on B_2 coordinate axes, I is the identity matrix, and C^{B1}_{B2} is a direction cosine matrix that transforms vector components from their values in non-rotating (inertial) coordinates B_2 to their values in inertial coordinates B_1.

Since non-rotating frames B_1 and B_2 are defined as aligned with the rotating B frame at time instants 1 and 2, we can calculate the change in B frame values of a vector during the t_1 to t_2 time interval as the difference between the B_1 and B_2 projected values. Thus, for particular terms in (5),

$$\underline{x}^{B2}_{p_2/i} - \underline{x}^{B1}_{p_1/i} \equiv \Delta\underline{\chi}^{B}_{p/i} \qquad \underline{x}^{B2}_{i\,2/a} - \underline{x}^{B1}_{i1/a} \equiv \Delta\underline{\chi}^{B}_{i/a} \tag{6}$$

where from t_1 to t_2 , $\Delta\underline{\chi}^{B}_{p/i}$ is the change in the distance vector from observation point i to point p in the rotating B frame (superscript), and $\Delta\underline{\chi}^{B}_{i/a}$ is the change in the distance vector from observation point a to point i as measured at point a in the rotating B frame. We also note that $C^{B1}_{B2} - I$ in (5) represents the change in the C^{B1}_{B} direction cosine matrix from its identity value at t_1 (when $B = B_1$) to its C^{B1}_{B2} value at t_2. For the angular rotation over t_1 to t_2, $C^{B1}_{B2} - I$ can be

equated to the equivalent rotation angle vector $\Delta\underline{\theta}_{IB}^{B}$ which for small angular rotations approximates as in [8 Sect 3.5.2]:

$$C_{B_2}^{B_1} - I \approx \left(\Delta\underline{\theta}_{IB}^{B}\times\right) \tag{7}$$

where the *IB* subscript indicates the angular rotation of frame *B* from its orientation parallel to non-rotating inertial frame B_1 to its orientation parallel to non-rotating inertial frame B_2. Substituting (6) and (7) in (5) obtains

$$\Delta\underline{x}_{p/i}^{B_1} = \Delta\underline{\chi}_{p/i}^{B} + \Delta\underline{\theta}_{IB}^{B}\times\underline{x}_{p_2/i}^{B_2} \qquad \Delta\underline{x}_{i/a}^{B_1} = \Delta\underline{\chi}_{i/a}^{B} + \Delta\underline{\theta}_{IB}^{B}\times\underline{x}_{i_2/a}^{B_2} \tag{8}$$

We then let the Δ changes become very small so that during the t_1 to t_2 time interval, Eq. (8) vector projections in the B_1 and B_2 frames can be approximated by their projections in the *B* frame in general, and the positions of points *p* and *i* at time instant t_2 can be approximated by their positions in general: $\underline{x}_{p_2/i}^{B_2} \to \underline{x}_{p/i}^{B}$, $\underline{x}_{i_2/a}^{B_2} \to \underline{x}_{i/a}^{B}$, $\Delta\underline{x}_{p/i}^{B_1} \to \Delta\underline{x}_{p/i}^{B}$, $\Delta\underline{x}_{i/a}^{B_1} \to \Delta\underline{x}_{i/a}^{B}$. Thus, (8) becomes

$$\Delta\underline{x}_{p/i}^{B} = \Delta\underline{\chi}_{p/i}^{B} + \Delta\underline{\theta}_{IB}^{B}\times\underline{x}_{p/i}^{B} \qquad \Delta\underline{x}_{i/a}^{B} = \Delta\underline{\chi}_{i/a}^{B} + \Delta\underline{\theta}_{IB}^{B}\times\underline{x}_{i/a}^{B} \tag{9}$$

Finally, since all vectors in (9) are now defined in *B* frame coordinates, we can dispense with the superscript notation to obtain the simplified form

$$\Delta\underline{x}_{p/i} = \Delta\underline{\chi}_{p/i} + \Delta\underline{\theta}\times\underline{x}_{p/i} \qquad \Delta\underline{x}_{i/a} = \Delta\underline{\chi}_{i/a} + \Delta\underline{\theta}\times\underline{x}_{i/a} \tag{10}$$

where $\Delta\underline{\theta}$ is the angular rotation of the body relative to non-rotating coordinates, and where during the $\Delta\underline{\theta}$ rotation, $\Delta\underline{\chi}_{p/i}$ is the position change of point *p* observed at point *i* in rotating coordinates, $\Delta\underline{x}_{p/i}$ is the position change of point *p* observed at point *i* in a non-rotating coordinate frame that is instantaneously aligned with the rotating frame, $\Delta\underline{\chi}_{i/a}$ is the position change of point *i* observed at point *a* in rotating coordinates, and $\Delta\underline{x}_{i/a}$ is the position change of point *i* observed at point *a* in a non-rotating coordinate frame that is instantaneously aligned with the rotating frame. Substituting $\Delta\underline{x}_{p/i}$ and $\Delta\underline{x}_{i/a}$ from (10) into (3) then obtains the general result:

$$\Delta\underline{x}_{p/a} = \Delta\underline{\chi}_{p/i} + \Delta\underline{\theta}\times\underline{x}_{p/i} + \Delta\underline{\chi}_{i/a} + \Delta\underline{\theta}\times\underline{x}_{i/a} \tag{11}$$

Relativity theory deals with variations from traditional Galilean kinematics when observations of distant events are made by observers travelling relative to one another [3 Chpt V1 Sect 2; 4; 9]. In the current development, (3) fits into this category because it involves

kinematic measurements made at point *a* (i.e., of distant events $\Delta\underline{x}_{p/a}$ and $\Delta\underline{x}_{i/a}$) and their relationship with a measurement made at point *i* (i.e., $\Delta\underline{x}_{p/i}$), point *i* being in motion relative to point *a*. But, Appendix A shows that (3) is identical to what would be obtained from Relativity theory when the distance travelled by observation point *i* relative to observation point *a* (i.e., $\left|\Delta\underline{x}_{i/a}\right|$) is small compared to the distance a photon would travel (at the speed of light) over the time interval for the $\Delta\underline{x}_{i/a}$ motion. On the other hand, Relativity theory does not apply for each of the $\Delta\underline{x}_{p/i}$ and $\Delta\underline{x}_{i/a}$ expressions in (10) substituted in (3) because each is derived from measurements made separately at either the *a* or *i* observation points. Thus, under normal operating conditions, (11) derived from (10) and (3), is generally compatible with both Galilean/Newtonian and Relativity kinematic theory.

APPLICATION TO A RIGID BODY AND SELECTION OF A PARTICULAR OBSERVATION POINT

Anticipating its application to optical gyros, we first specialize observation point *i* to be located at the starting point of the small $\Delta\underline{x}_{p/i}$ motion, hence,

$$\underline{x}_{p/i} \approx 0 \tag{12}$$

Thus (11) and the $\Delta\underline{x}_{p/i}$ expression in (10) simplify to

$$\Delta\underline{x}_{p/i} = \Delta\underline{\chi}_{p/i} \qquad \Delta\underline{x}_{p/a} = \Delta\underline{\chi}_{p/i} + \Delta\underline{\chi}_{i/a} + \Delta\underline{\theta} \times \underline{x}_{i/a} \tag{13}$$

For a rigid rotating body, there is no movement between points fixed within the body. Thus, if we now define points *a* and *i* to be fixed within the rotating body, $\Delta\underline{\chi}_{i/a} = 0$, and (13) reduces to

$$\Delta\underline{x}_{p/i} = \Delta\underline{\chi}_{p/i} \qquad \Delta\underline{x}_{p/a} = \Delta\underline{\chi}_{p/i} + \Delta\underline{\theta} \times \underline{x}_{i/a} \tag{14}$$

Eqs. (14) are fundamental relationships describing position changes $\Delta\underline{x}_{p/i}$, $\Delta\underline{x}_{p/a}$ of an arbitrary point *p* that would be measured in non-rotating coordinates at points *i* and *a* within the body, as functions of $\Delta\underline{\chi}_{p/i}$, the *p* motion that would be measured in rotating coordinates at point *i* within the body, the differential angular rotation $\Delta\underline{\theta}$ of the body relative to inertial space during the *p* motion, and the distance vector $\underline{x}_{i/a}$ from point *a* to point *i*. Since (14) was derived from (12) and (10), it is also compatible with traditional vector kinematic theory, and under normal operating conditions, Relativity theory.

The relationship between $\Delta\underline{x}_{p/a}$ and $\Delta\underline{\chi}_{p/i}$ magnitudes will be subsequently useful, and derives from the dot product of $\Delta\underline{x}_{p/a}$ in (14) with itself:

$$\begin{aligned}\Delta\underline{x}_{p/a}\,.\,\Delta\underline{x}_{p/a} &= \left(\Delta\underline{\chi}_{p/i}+\Delta\underline{\theta}\times\underline{x}_{i/a}\right).\left(\Delta\underline{\chi}_{p/i}+\Delta\underline{\theta}\times\underline{x}_{i/a}\right)\\ &= \Delta\underline{\chi}_{p/i}\,.\,\Delta\underline{\chi}_{p/i}+2\Delta\underline{\chi}_{p/i}\,.\left(\Delta\underline{\theta}\times\underline{x}_{i/a}\right)+\left(\Delta\underline{\theta}\times\underline{x}_{i/a}\right).\left(\Delta\underline{\theta}\times\underline{x}_{i/a}\right)\\ &\approx \Delta\underline{\chi}_{p/i}\,.\,\Delta\underline{\chi}_{p/i}+2\Delta\underline{\chi}_{p/i}\,.\left(\Delta\underline{\theta}\times\underline{x}_{i/a}\right)\end{aligned} \tag{15}$$

Dividing (15) by $\Delta\underline{\chi}_{p/i}\,.\,\Delta\underline{\chi}_{p/i}$ finds

$$\frac{\Delta\underline{x}_{p/a}\,.\,\Delta\underline{x}_{p/a}}{\Delta\underline{\chi}_{p/i}\,.\,\Delta\underline{\chi}_{p/i}} = 1+2\frac{\Delta\underline{\chi}_{p/i}\,.\left(\Delta\underline{\theta}\times\underline{x}_{i/a}\right)}{\Delta\underline{\chi}_{p/i}\,.\,\Delta\underline{\chi}_{p/i}} \tag{16}$$

Recognizing that the magnitudes of $\Delta\underline{x}_{p/a}$ and $\Delta\underline{\chi}_{p/i}$ are the square roots of $\Delta\underline{x}_{p/a}\,.\,\Delta\underline{x}_{p/a}$ and $\Delta\underline{\chi}_{p/i}\,.\,\Delta\underline{\chi}_{p/i}$ then obtains for the square root of (16):

$$\frac{\left|\Delta\underline{x}_{p/a}\right|}{\left|\Delta\underline{\chi}_{p/i}\right|} = \sqrt{\frac{\Delta\underline{x}_{p/a}\,.\,\Delta\underline{x}_{p/a}}{\Delta\underline{\chi}_{p/i}\,.\,\Delta\underline{\chi}_{p/i}}} \approx 1+\frac{\Delta\underline{\chi}_{p/i}\,.\left(\Delta\underline{\theta}\times\underline{x}_{i/a}\right)}{\left|\Delta\underline{\chi}_{p/i}\right|\left|\Delta\underline{\chi}_{p/i}\right|} = 1+\frac{\left(\underline{x}_{i/a}\times\Delta\underline{\chi}_{p/i}\right)\cdot\Delta\underline{\theta}}{\left|\Delta\underline{\chi}_{p/i}\right|^2} \tag{17}$$

WAVELENGTH EQUIVALENCE

Now consider that *p* represents a point in a monochromatic light wave travelling past point *i*, and that in the rotating frame, $\Delta\underline{\chi}_{p/i}$ represents the distance between successive waves passing by *i*. Then $\Delta\underline{\chi}_{p/i}=\lambda_{p/i}\,\underline{u}_i$ where $\lambda_{p/i}$ is the length of the *p* light wave (i.e., the "wavelength") at point *i*, $\underline{u}_{p/i}$ is a unit vector along the *p* wave travel direction at point *i*, and $\left|\Delta\underline{\chi}_{p/i}\right|=\lambda_{p/i}$. Thus, (17) is equivalently:

$$\begin{aligned}\frac{\left|\Delta\underline{x}_{p/a}\right|}{\left|\Delta\underline{\chi}_{p/i}\right|} &= \frac{\left|\Delta\underline{x}_{p/a}\right|}{\lambda_{p/i}} = 1+\frac{\left[\underline{x}_{i/a}\times\left(\lambda_{p/i}\,\underline{u}_{p/i}\right)\right]\cdot\Delta\underline{\theta}}{\lambda_{p/i}^2}\\ &= 1+\frac{\left(\underline{x}_{i/a}\times\underline{u}_{p/i}\right)\cdot\Delta\underline{\theta}}{\lambda_{p/i}} = 1+\left(\underline{x}_{i/a}\times\underline{u}_{p/i}\right).\frac{\Delta\underline{\theta}}{\lambda_{p/i}}\end{aligned} \tag{18}$$

Note, however, that the $\left|\Delta \underline{x}_{p/a}\right|$ measurement is independent of rotation (i.e., relative to point *i* motion), hence, it would be the same no matter the value of $\Delta\underline{\theta}$. Thus, if we define λ_{0_p} as the value of $\lambda_{p/i}$ under zero $\Delta\underline{\theta}$, we see from (18) that $\left|\Delta \underline{x}_{p/a}\right| = \lambda_{0_p}$, and (18) becomes:

$$\frac{\lambda_{0_p}}{\lambda_{p/i}} = 1 + \left(\underline{x}_{i/a} \times \underline{u}_{p/i}\right) \cdot \frac{\Delta\underline{\theta}}{\lambda_{p/i}} \tag{19}$$

We also define $\Delta t_{p/i}$ as the time interval for a *p* wave at point *i* to translate through a wavelength of distance $\left|\Delta \underline{\chi}_{p/i}\right| = \lambda_{p/i}$ relative to the rotating rigid body. The *p* wave speed $V_{p/i}$ relative to the rotating body at point *i* would then be $\left|\Delta \underline{\chi}_{p/i}\right| / \Delta t_{p/i}$ or equivalently, $\left|\Delta \underline{\chi}_{p/i}\right| = V_{p/i}\ \Delta t_{p/i}$. Hence, $\left|\Delta \underline{\chi}_{p/i}\right| = \lambda_{p/i} = V_{p/i}\ \Delta t_{p/i}$, and substitution in (19) finds

$$\frac{\lambda_{0_p}}{\lambda_{p/i}} = 1 + \left(\underline{x}_{i/a} \times \underline{u}_{p/i}\right) \cdot \frac{\Delta\underline{\theta}}{\lambda_{p/i}}$$

$$= 1 + \left(\underline{x}_{i/a} \times \underline{u}_{p/i}\right) \cdot \frac{\Delta\underline{\theta}}{V_{p/i}\,\Delta t_{p/i}} = 1 + \frac{\left(\underline{x}_{i/a} \times \underline{u}_{p/i}\right)}{V_{p/i}} \cdot \frac{\Delta\underline{\theta}}{\Delta t_{p/i}} \tag{20}$$

$$\text{where} \quad V_{p/i} \equiv \left|\Delta \underline{\chi}_{p/i}\right| / \Delta t_{p/i}$$

DIFFERENTIAL FORMS

The remainder of the article will deal with equivalent differential forms for which the small Δ changes in (14) and (20) become infinitesimally small. Thus:

$$d\underline{x}_{p/i} = d\underline{\chi}_{p/i} \qquad d\underline{x}_{p/a} = d\underline{\chi}_{p/i} + d\underline{\theta} \times \underline{x}_{i/a} \qquad V_{p/i} \equiv \left|d\underline{\chi}_{p/i}\right| / dt_{p/i}$$

$$\frac{\lambda_{0_p}}{\lambda_{p/i}} = 1 + \frac{\left(\underline{x}_{i/a} \times \underline{u}_{p/i}\right)}{V_{p/i}} \cdot \frac{d\underline{\theta}}{dt_{p/i}} \tag{21}$$

where during the $dt_{p/i}$ differential time interval, $V_{p/i}$ is the instantaneous speed of the *p* wave relative to the rotating body at point *i*, $d\underline{\theta}$ is the differential angular rotation of the body relative to non-rotating space, $d\underline{x}_{p/i}$, $d\underline{x}_{p/a}$ are differential distance vector movements of point *p* as viewed from points *i* and *a* in non-rotating inertial coordinates, and $d\underline{\chi}_{p/i}$ is the differential distance vector movement of point *p* as viewed from point *i* in rotating body coordinates.

THE EFFECT OF RELATIVITY

The derivations leading to (21) have been based on classical Euclidean vector geometry. To continue, we now incorporate a basic precept of Relativity theory: that the speed of light is the same constant when measured at any point in non-rotating inertial space [2 Part 1 Chpt 11]. Thus, since $d\underline{x}_{p/i}$ is the differential distance movement of *p* in non-rotating space at point *i*, and since $d\underline{x}_{p/i}$ occurs over differential time interval $dt_{p/i}$, it follows that the speed of *p* over $dt_{p/i}$ will be the speed of light *c*, i.e., $\left|d\underline{x}_{p/i}\right| / dt_{p/i} = c$. But from (21), $d\underline{x}_{p/i} = d\underline{\chi}_{p/i}$, hence, $\left|d\underline{\chi}_{p/i}\right| = \left|d\underline{x}_{p/i}\right|$, and $\left|d\underline{\chi}_{p/i}\right| / dt_{p/i} = \left|d\underline{x}_{p/i}\right| / dt_{p/i}$. We also know from (21) that $V_{p/i} \equiv \left|d\underline{\chi}_{p/i}\right| / dt_{p/i}$. It follows then that $V_{p/i} = \left|d\underline{x}_{p/i}\right| / dt_{p/i} = c$. Thus, relative to the rotating body, the magnitude of the *p* velocity at point *i* will also be the speed of light *c*. This finding is the fundamental basis for optical gyros being able to measure angular rotation relative to non-rotating inertial space. For $dt_{p/i}$ redefined to be a specified differential time increment *dt* (relative to the rotating body), the finding directly links $\left|d\underline{\chi}_{p/i}\right|$ to *dt*. Then $\left|d\underline{\chi}_{p/i}\right|$ and $\lambda_{0_p} / \lambda_{p/i}$ in (21) with $V_{p/i} = c$ gives the important result:

$$\left|d\underline{\chi}_{p/i}\right| = c\,dt \qquad \frac{1}{\lambda_{p/i}} = \frac{1}{\lambda_{0_p}}\left[1 + \frac{\left(\underline{x}_{i/a} \times \underline{u}_{p/i}\right)}{c} \cdot \underline{\omega}\right] \qquad \underline{\omega} \equiv \frac{d\underline{\theta}}{dt} \qquad (22)$$

where $\underline{\omega}$ is the instantaneous angular rate, and because angular rotation $d\underline{\theta}$ has been defined to be relative to non-rotating inertial space, $\underline{\omega}$ is also relative to non-rotating inertial space. Eq. (22) is now in a convenient form for optical gyro application.

APPLICATION TO OPTICAL GYROS

Optical gyros create two oppositely directed but superimposed monochromatic light waves that traverse a closed-optical path, one (as before) identified as a *p* wave viewed from a point *i* in the waveguide, the oppositely directed wave as *q* viewed from a point *j* in the waveguide. The direction for *p* wave travel in the waveguide at point *i* is then defined $\underline{u}_{p/i}$ (as before), and similarly, $\underline{u}_{q/j}$ is defined as a unit vector in the *q* wave travel direction at point *j* in the waveguide. To distinguish the opposite travel directions of the waves, we then designate $\underline{u}_i$ as a general waveguide direction unit vector defined to be parallel to the *p* wave travel vector $\underline{u}_{p/i}$ at point *i* (i.e., $\underline{u}_i \equiv \underline{u}_{p/i}$). If the *p* wave was at point *j* in the waveguide, $\underline{u}_j$ would represent the *p* wave direction $\underline{u}_{p/j}$ (i.e., $\underline{u}_j = \underline{u}_{p/j}$). Then, to represent the opposite direction of *q* wave travel

at point j, we assign $\underline{u}_{q/j} = -\underline{u}_j$. Finally, as will be justified subsequently for particular optical gyro configurations, the p and q wavelengths under zero angular change will be the same λ_0 value (i.e., $\lambda_{0_q} = \lambda_{0_p} = \lambda_0$). Based on these observations, general Eqs. (22) then give for the p and q waves:

$$\left|d\underline{\chi}_{p/i}\right| = c\,dt = ds_p = dL \qquad \frac{1}{\lambda_{p/i}} = \frac{1}{\lambda_0}\left[1 + \frac{\left(\underline{x}_{i/a} \times \underline{u}_i\right)}{c} \cdot \underline{\omega}\right]$$
$$\left|d\underline{\chi}_{q/j}\right| = c\,dt = ds_q = dL \qquad \frac{1}{\lambda_{q/j}} = \frac{1}{\lambda_0}\left[1 - \frac{\left(\underline{x}_{j/a} \times \underline{u}_j\right)}{c} \cdot \underline{\omega}\right] \tag{23}$$

where ds_p, ds_q are dL the distance moved by the p, q waves (relative to the rotating waveguide) during the infinitesimal dt time interval (relative to the rotating waveguide. Note in (23) that by virtue of the p and q waves both travelling at the speed of light c relative to the rotating gyro, the ds_p, ds_q motion over the same time interval dt equal the same distance dL in magnitude, even though they represent p, q wave movement at different i, j locations in the waveguide.

The difference in p, q wave wavelengths in (23) is the mechanism for measuring angular change in optical gyros. To understand how, the light wave structure and means for measurement will now be addressed.

LIGHT WAVE EQUIVALENCE

Consider common point l where the "clockwise" p wave and "counterclockwise" q wave first enter the waveguide (at past time $\tau = 0$). Further, consider point m in the "readout zone" on the waveguide at current time $\tau = T$ where the p and q waves combine to generate an output measurement.

For the p wave, the phase at point m compared with the phase along the wave at another point l would be at the same instant of time:

$$\phi(p,m) = \phi(p,l) + \int_{s_p=0}^{s_p=L} \frac{2\pi}{\lambda_{s_p}} ds_p \tag{24}$$

where λ_{s_p} is the wave length at distance s_p from point l, $\phi(p,l)$ and $\phi(p,m)$ are the wave phases at point l and m, and L is the linear wave path distance from l to m. For a sinusoidal p wave, the corresponding wave "height" at points l and m would be

$$g(p,l) = B\sin\phi(p,l) \qquad g(p,m) = B\sin\phi(p,m) \tag{25}$$

where B is the p wave amplitude. For constant angular rate $\underline{\omega}$ (relative to non-rotating inertial space), substitution for λ_{sp} from (23) in (24) then finds

$$\phi(p,m) = \phi(p,l) + \frac{2\pi}{\lambda_0} \int_{s_p=0}^{s_p=L} \left[1 + \frac{\left(\underline{x}_{i/a} \times \underline{u}_i \right)}{c} \cdot \underline{\omega} \right] ds_p \tag{26}$$

where $\underline{x}_{i/a}$, $\underline{u}_i$ are the (23) values at distance s_p from l. For the q wave, the equivalent of (25) – (26) would be

$$\phi(q,m) = \phi(q,l) + \frac{2\pi}{\lambda_0} \int_{s_q=0}^{s_q=L} \left[1 - \frac{\left(\underline{x}_{j/a} \times \underline{u}_j \right)}{c} \cdot \underline{\omega} \right] ds_q \tag{27}$$

$$g(q,l) = B \sin \phi(q,l) \qquad g(q,m) = B \sin \phi(q,m)$$

Eqs. (26) with (25) and (27) are based on constant angular rate $\underline{\omega}$, hence, the $\phi(p,m)$, $\phi(q,m)$ integrals are a function of $\underline{x}_{i/a}$ locations along the light wave between points l and m. Alternatively, the (25) and (27) integrals can be performed in steps at points along the wave path that a wave front would move (at the speed of light) from point l. As an example, for a p wave front that has moved a distance s_{p1} over time interval τ from point l (i.e., $s_{p1} = c\tau$), the p wave phase would be

$$\phi(p,s_{p1}) = \phi(p,l) + \frac{2\pi}{\lambda_0} \int_{s_p=0}^{s_p=c\tau} \left[1 + \frac{\left(\underline{x}_{i/a} \times \underline{u}_i \right)}{c} \cdot \underline{\omega} \right] ds_p \tag{28}$$

At another point s_{p2} ahead of s_{p1} by time interval $d\tau$, the phase would be

$$\phi(p,s_{p2}) = \phi(p,l) + \frac{2\pi}{\lambda_0} \int_{s_p=0}^{s_p=c(\tau+d\tau)} \left[1 + \frac{\left(\underline{x}_{i/a} \times \underline{u}_i \right)}{c} \cdot \underline{\omega} \right] ds_p$$

$$= \phi(p,l) + \frac{2\pi}{\lambda_0} \int_{s_p=0}^{s_p=c\tau} \left[1 + \frac{\left(\underline{x}_{i/a} \times \underline{u}_i \right)}{c} \cdot \underline{\omega} \right] ds_p + \frac{2\pi}{\lambda_0} \int_{s_p=c\tau}^{s_p=c(\tau+d\tau)} \left[1 + \frac{\left(\underline{x}_{i/a} \times \underline{u}_i \right)}{c} \cdot \underline{\omega} \right] ds_p \tag{29}$$

$$= \phi(p,s_{p1}) + \frac{2\pi}{\lambda_0} \int_{s_p=c\tau}^{s_p=c(\tau+d\tau)} \left[1 + \frac{\left(\underline{x}_{i/a} \times \underline{u}_i \right)}{c} \cdot \underline{\omega} \right] ds_p \approx \phi(p,s_1) + \frac{2\pi}{\lambda_0} \left[1 + \frac{\left(\underline{x}_{i/a} \times \underline{u}_i \right)}{c} \cdot \underline{\omega} \right] cd\tau$$

$$= \phi(p,s_{p1}) + \frac{2\pi}{\lambda_0} \left[cd\tau + \left(\underline{x}_{i/a} \times \underline{u}_i \right) \cdot \underline{\omega}\, d\tau \right]$$

With rearrangement and generalization, (29) becomes

$$d\phi(s_p) \equiv \phi(p, s_{p2}) - (\phi(p, s_{p1}) = \frac{2\pi}{\lambda_0}\left\{c + \left[\underline{x}_{i/a}(\tau) \times \underline{u}_i(\tau)\right] . \underline{\omega}\right\} d\tau \qquad (30)$$

where $d\phi(s_p)$ is the p wave differential phase change (relative to point l) incurred as the wave front moved at light speed c over distance $ds_p = cd\tau$ from point s_{p1} to s_{p2} over the $d\tau$ time interval, and where $\underline{x}_{i/a}(\tau)$, $\underline{u}_i(\tau)$ are $\underline{x}_{i/a}$, $\underline{u}_i$ at distance $c\tau$ along the wave path where the p wave front has moved at the speed of light (over time interval τ) from point l. Then the cumulative phase of (30) at point m and at time $\tau = T$ would be

$$\phi(T)_{p/m} = \phi(p,l) + \frac{2\pi}{\lambda_0}\left\{cT + \int_{\tau=0}^{\tau=T}\left[\underline{x}_{i/a}(\tau) \times \underline{u}_i(\tau)\right] . \underline{\omega} d\tau\right\} \qquad (31)$$

where T is the time interval for the wave front to move from point l to point m over distance L at the speed of light (i.e., $L = cT$), and $\phi(T)_{p/m}$ is the p wave phase at readout zone point m at current time T. Similarly from (23), for q wave front movement to point m along its wave path over the same distance L (from past time $\tau = 0$ to current time $\tau = T$):

$$\phi(T)_{q/m} = \phi(q,l) + \frac{2\pi}{\lambda_0}\left\{cT - \int_{\tau=0}^{\tau=T}\left[\underline{x}_{j/a}(\tau) \times \underline{u}_j(\tau)\right] . \underline{\omega}\, d\tau\right\} \qquad (32)$$

The interesting thing about (30) - (32) is that they would also be true if $\underline{\omega}$ varied with time, equaling the value at time τ where the wave front had travelled the distance $c\tau$ from point l on the wave path. Thus, we can also use (31) and (32) to represent p and q wave phases for a time varying $\underline{\omega}$. With (31) and (32) substituted in (25) - (27), the p and q wave phases at readout zone point m at current time T would then become for time varying $\underline{\omega}$:

$$\begin{aligned}
\phi(T)_{p/m} &= \phi(p,l) + \frac{2\pi}{\lambda_0}\left\{cT + \int_{\tau=0}^{\tau=T}\left[\underline{x}_{i/a}(\tau) \times \underline{u}_i(\tau)\right] . \underline{\omega}(\tau) d\tau\right\} \\
\phi(T)_{q/m} &= \phi(q,l) + \frac{2\pi}{\lambda_0}\left\{cT - \int_{\tau=0}^{\tau=T}\left[\underline{x}_{j/a}(\tau) \times \underline{u}_j(\tau)\right] . \underline{\omega}(\tau)\, d\tau\right\}
\end{aligned} \qquad (33)$$

where the angular rate time dependence has now been more clearly delineated as $\underline{\omega}(\tau)$. Under accumulating differential rotation, (33) shows that the p wave phase will increase by

$\frac{2\pi}{\lambda_0}\int_{\tau=0}^{\tau=T}\left[\underline{x}_{i/a}(\tau)\times\underline{u}_i(\tau)\right].\underline{\omega}(\tau)\,d\tau$, and the q wave phase will decrease by $\frac{2\pi}{\lambda_0}\int_{\tau=0}^{\tau=T}\left[\underline{x}_{j/a}(\tau)\times\underline{u}_j(\tau)\right].\underline{\omega}(\tau)\,d\tau$. The resulting phase difference at time T in the gyro "readout zone" provides the measurement of angular rotation for output.

INPUT AXIS DEFINITION

The integral terms in Eqs. (33) show that $\phi(T)_{p/m}$ and $\phi(T)_{q/m}$ measure the integrated component of $\underline{\omega}(t)$ along the $\left[\underline{x}_{i/a}(\tau)\times\underline{u}_i(\tau)\right]$ and $\left[\underline{x}_{j/a}(\tau)\times\underline{u}_j(\tau)\right]$ vectors. We define the $\underline{\omega}(\tau)$ input axis at points i and j as unit vectors $\underline{u}_{Inpt_i}(\tau)$, $\underline{u}_{Inpt_j}(\tau)$ along $\left[\underline{x}_{i/a}(\tau)\times\underline{u}_i(\tau)\right]$, $\left[\underline{x}_{j/a}(\tau)\times\underline{u}_j(\tau)\right]$:

$$\underline{u}_{Inpt_i}(t)\equiv\frac{\underline{x}_{i/a}(\tau)\times\underline{u}_i(\tau)}{\left|\underline{x}_{i/a}(\tau)\times\underline{u}_i(\tau)\right|}\quad x_{i/a_\perp}\equiv\left|\underline{x}_{i/a}(\tau)\times\underline{u}_i(\tau)\right|\ \rightarrow\ \underline{x}_{i/a}(\tau)\times\underline{u}_i(\tau)=x_{i/a_\perp}(\tau)\,\underline{u}_{Inpt_i}(\tau)$$
$$\underline{u}_{Inpt_j}(t)\equiv\frac{\underline{x}_{j/a}(\tau)\times\underline{u}_j(\tau)}{\left|\underline{x}_{j/a}(\tau)\times\underline{u}_j(\tau)\right|}\quad x_{j/a_\perp}\equiv\left|\underline{x}_{j/a}(\tau)\times\underline{u}_j(\tau)\right|\ \rightarrow\ \underline{x}_{j/a}(\tau)\times\underline{u}_j(\tau)=x_{j/a_\perp}(\tau)\,\underline{u}_{Inpt_j}(\tau)\qquad(34)$$

where $x_{i/a_\perp}(\tau)$, $x_{j/a_\perp}(\tau)$ are components of $\underline{x}_{i/a}(\tau)$, $\underline{x}_{j/a}(\tau)$ perpendicular to the waveguide direction vectors at points i, j. Then (33) becomes

$$\phi(T)_{p/m}=\phi(p,l)+\frac{2\pi}{\lambda_0}\left[cT+\int_{\tau=0}^{\tau=T}x_{i/a_\perp}(\tau)\,\underline{u}_{Inpt_i}(\tau).\underline{\omega}(\tau)\,d\tau\right]$$
$$\phi(T)_{q/m}=\phi(q,l)+\frac{2\pi}{\lambda_0}\left[cT-\int_{\tau=0}^{\tau=T}x_{j/a_\perp}(\tau)\,\underline{u}_{Inpt_j}(\tau).\underline{\omega}(\tau)\,d\tau\right]\qquad(35)$$

COMBINED OPPOSITELY DIRECTED WAVES IN THE READOUT ZONE

Now consider the wave height at point m at time $\Delta\tau$, a small time variation from time $\tau=T$. As both the p and q waves pass by point m, they then will generate sinusoidal outputs at point m of the form

$$g(T+\Delta\tau)_{p/m}=B\sin\left[\frac{2\pi}{\lambda_m}c\Delta\tau+\phi(T)_{p/m}\right]\qquad g(T+\Delta\tau)_{q/m}=B\sin\left[\frac{2\pi}{\lambda_m}c\Delta\tau+\phi(T)_{q/m}\right]\quad(36)$$

with $\phi(T)_{p/m}$ and $\phi(T)_{q/m}$ as defined in (35). Note: Eqs. (36) are based on the very good approximation that $\Delta\tau$ is very small, thus, angular rate can be considered constant, and λ_m will also be constant - see (23) and note the very small dependence of λ_m on $\underline{\omega}(\tau)$.

Because the *p* and *q* waves occupy the same space in the waveguide at point *m*, their (36) wave functions at common "readout zone" point *m* will add at time $\tau = T + \Delta\tau$ to form

$$\begin{aligned} h(T+\Delta\tau)_m &\equiv g(T+\Delta\tau)_{p/m} + g(T+\Delta\tau)_{q/m} \\ &= B\sin\left[\frac{2\pi}{\lambda_m}c\Delta\tau + \phi(T)_{p/m}\right] + B\sin\left[\frac{2\pi}{\lambda_m}c\Delta\tau + \phi(T)_{q/m}\right] \end{aligned} \tag{37}$$

or with (33):

$$\begin{aligned} h(T+\Delta\tau)_m &= B\sin\left\langle \frac{2\pi}{\lambda_m}c\Delta\tau + \phi(p,l) + \frac{2\pi}{\lambda_0}\left\{cT + \int_{\tau=0}^{\tau=T}\left[\underline{x}_{i/a}(\tau)\times\underline{u}_i(\tau)\right].\underline{\omega}(\tau)\,d\tau\right\}\right\rangle \\ &\quad + B\sin\left\langle \frac{2\pi}{\lambda_m}c\Delta\tau + \phi(q,l) + \frac{2\pi}{\lambda_0}\left\{cT - \int_{\tau=0}^{\tau=T}\left[\underline{x}_{j/a}(\tau)\times\underline{u}_j(\tau)\right].\underline{\omega}(\tau)\,d\tau\right\}\right\rangle \\ &= 2B\sin\frac{1}{2}\left\langle \begin{array}{l} \dfrac{2\pi}{\lambda_m}c\Delta\tau + \phi(p,l) + \dfrac{2\pi}{\lambda_0}\left\{cT + \displaystyle\int_{\tau=0}^{\tau=T}\left[\underline{x}_{i/a}(\tau)\times\underline{u}_i(\tau)\right].\underline{\omega}(\tau)\,d\tau\right\} \\ +\dfrac{2\pi}{\lambda_m}c\Delta\tau + \phi(q,l) + \dfrac{2\pi}{\lambda_0}\left\{cT - \displaystyle\int_{\tau=0}^{\tau=T}\left[\underline{x}_{j/a}(\tau)\times\underline{u}_j(\tau)\right].\underline{\omega}(\tau)\,d\tau\right\} \end{array}\right\rangle \times \\ &\quad \cos\frac{1}{2}\left\langle \begin{array}{l} \dfrac{2\pi}{\lambda_m}c\Delta\tau + \phi(p,l) + \dfrac{2\pi}{\lambda_0}\left\{cT + \displaystyle\int_{\tau=0}^{\tau=T}\left[\underline{x}_{i/a}(\tau)\times\underline{u}_i(\tau)\right].\underline{\omega}(\tau)\,d\tau\right\} \\ -\dfrac{2\pi}{\lambda_m}c\Delta\tau - \phi(q,l) - \dfrac{2\pi}{\lambda_0}\left\{cT - \displaystyle\int_{\tau=0}^{\tau=T}\left[\underline{x}_{j/a}(\tau)\times\underline{u}_j(\tau)\right].\underline{\omega}(\tau)\,d\tau\right\} \end{array}\right\rangle \\ &= 2B\sin\left\{ \begin{array}{c} \dfrac{2\pi c}{\lambda_m}\Delta\tau + \dfrac{2\pi c}{\lambda_0}T + \dfrac{\phi(p,l)+\phi(q,l)}{2} \\ +\dfrac{\pi}{\lambda_0}\displaystyle\int_{\tau=0}^{\tau=T}\left[x_{i/a_\perp}(\tau)\,\underline{u}_{Inpt_i}(\tau) - x_{j/a_\perp}(\tau)\,\underline{u}_{Inpt_j}(\tau)\right].\underline{\omega}(\tau)\,d\tau \end{array}\right\}\times \\ &\quad \cos\left\{\frac{\phi(p,l)-\phi(q,l)}{2} + \frac{\pi}{\lambda_0}\int_{\tau=0}^{\tau=T}\left[x_{i/a_\perp}(\tau)\,\underline{u}_{Inpt_i}(\tau) + x_{j/a_\perp}(\tau)\,\underline{u}_{Inpt_j}(\tau)\right].\underline{\omega}(\tau)\,d\tau\right\} \end{aligned} \tag{38}$$

where $h(T+\Delta\tau)_m$ is a combined *p* and *q* wave function at point *m* in the readout zone at time $\tau = T + \Delta\tau$. (Note: Eq. (38) assumes that the $g(T+\Delta\tau)_{p/m}$ and $g(T+\Delta\tau)_{q/m}$ functions lie in the same plane around the waveguide at the same instant of time and space, so that they add

algebraically as shown. An important part of optical gyro design is based on meeting this requirement.)

The normalized power $W(T+\Delta\tau)_m$ in the combined (38) optical beam signal is proportional to the square of $h(T+\Delta\tau)_m$ in (38):

$$W(T+\Delta\tau)_m \equiv \frac{h(T+\Delta\tau)_m^2}{B^2}$$

$$= 4\sin^2\left\{\begin{array}{c}\dfrac{2\pi c}{\lambda_m}\Delta\tau + \dfrac{2\pi c}{\lambda_0}T + \dfrac{\phi(p,l)+\phi(q,l)}{2} \\ +\dfrac{\pi}{\lambda_0}\int\limits_{\tau=0}^{\tau=T}\left[x_{i/a_\perp}(\tau)\,\underline{u}_{Inpt_i}(\tau) - x_{j/a_\perp}(\tau)\,\underline{u}_{Inpt_j}(\tau)\right].\underline{\omega}(\tau)\,d\tau\end{array}\right\}\times \qquad (39)$$

$$\cos^2\left\{\frac{\phi(p,l)-\phi(q,l)}{2} + \frac{\pi}{\lambda_0}\int\limits_{\tau=0}^{\tau=T}\left[x_{i/a_\perp}(\tau)\,\underline{u}_{Inpt_i}(\tau) + x_{j/a_\perp}(\tau)\,\underline{u}_{Inpt_j}(\tau)\right].\underline{\omega}(\tau)\,d\tau\right\}$$

or with trigonometric expansion,

$$W(T+\Delta\tau)_m$$

$$= \left\langle 1-\cos\left\{\begin{array}{c}\dfrac{4\pi c}{\lambda_m}\Delta\tau + \dfrac{4\pi c}{\lambda_0}T + \left(\phi(p,l)+\phi(q,l)\right) \\ +\dfrac{2\pi}{\lambda_0}\int\limits_{\tau=0}^{\tau=T}\left[x_{i/a_\perp}(\tau)\,\underline{u}_{Inpt_i}(\tau) - x_{j/a_\perp}(\tau)\,\underline{u}_{Inpt_j}(\tau)\right].\underline{\omega}(\tau)\,d\tau\end{array}\right\}\right\rangle\times \qquad (40)$$

$$\left\langle 1+\cos\left\{\phi(p,l)-\phi(q,l)+\frac{2\pi}{\lambda_0}\int\limits_{\tau=0}^{\tau=T}\left[x_{i/a_\perp}(\tau)\,\underline{u}_{Inpt_i}(\tau) + x_{j/a_\perp}(\tau)\,\underline{u}_{Inpt_j}(\tau)\right].\underline{\omega}(\tau)\,d\tau\right\}\right\rangle$$

Eq. (40) describes the power that would be measured by a photo detector located at point *m* in the waveguide at time $T+\Delta\tau$, being simultaneously illuminated by the *p*, *q* light beams. The power magnitude is modulated at high frequency by the first cosine term. For a typical optical gyro wavelength $\lambda_m \approx \lambda_0$ of 0.63 microns (for a ring laser gyro), the modulation frequency $2c/\lambda_m$ in the (40) cosine term is high enough (2 × 3.0e8 / 0.63e-6 = 9.52 e14 Hz) to be eliminated by attenuation in the photo-detector/readout electronics. Thus, (40) simplifies to

$$W(T)_m = 1+\cos\left\{\begin{array}{c}\phi(p,l)-\phi(q,l) \\ +\dfrac{2\pi}{\lambda_0}\int\limits_{\tau=0}^{\tau=T}\left[x_{i/a_\perp}(\tau)\,\underline{u}_{Inpt_i}(\tau) + x_{j/a_\perp}(\tau)\,\underline{u}_{Inpt_j}(\tau)\right].\underline{\omega}(\tau)\,d\tau\end{array}\right\} \qquad (41)$$

where $W(T)_m$ is $W(T+\Delta\tau)_m$ at time $\tau = T$ (when $\Delta\tau = 0$).

Eq. (41) is the basis for the design of both ring laser and fiber optic gyros. It demonstrates that optical gyros are integrating instruments whose combined optical beam power $W(T)_m$ measures the integral of gyro input angular rate relative to non-rotating inertial space.

PLANAR WAVEGUIDES

For optical gyros having waveguides that lie in a single plane, $\underline{u}_{Inpt_i}(\tau)$ and $\underline{u}_{Inpt_j}(\tau)$ are parallel, both perpendicular to the waveguide plane, hence, $\underline{u}_{Inpt_i}(\tau) = \underline{u}_{Inpt_j}(\tau) = \underline{u}_{Inpt}$ where $\underline{u}_{Inpt}$ is a unit vector normal to the plane and is the gyro input axis for both the *p* and *q* waves. Then the integral term in (41) becomes

$$\begin{aligned}
&\frac{2\pi}{\lambda_0}\int_{\tau=0}^{\tau=T}\left[x_{i/a_\perp}(\tau)\,\underline{u}_{Inpt_i}(\tau) + x_{j/a_\perp}(\tau)\,\underline{u}_{Inpt_j}(\tau)\right].\underline{\omega}(\tau)\,d\tau \\
&= \frac{2\pi}{\lambda_0}\int_{\tau=0}^{\tau=T}\left[x_{i/a_\perp}(\tau)\,\underline{u}_{Inpt} + x_{j/a_\perp}(\tau)\,\underline{u}_{Inpt}\right].\underline{\omega}(\tau)\,d\tau \\
&= \frac{2\pi}{\lambda_0}\int_{\tau=0}^{\tau=T}\left[x_{i/a_\perp}(\tau) + x_{j/a_\perp}(\tau)\right]\underline{u}_{Inpt}.\underline{\omega}(\tau)\,d\tau \\
&= \frac{2\pi}{\lambda_0}\int_{\tau=0}^{\tau=T}\left[x_{i/a_\perp}(\tau) + x_{j/a_\perp}(\tau)\right]\omega(\tau)_{Inpt}\,d\tau
\end{aligned} \tag{42}$$

where $\omega(\tau)_{Inpt}$ is the component of $\underline{\omega}$ along the gyro $\underline{u}_{Inpt}$ input axis.

For the most common situation when the waveguide is in the shape of a regular polygon, a circle can be inscribed within the waveguide that is tangent to each side of the polygon. Then, the perpendicular distance from the center of the inscribed circle (the "centroid") to any side equals the radius of the inscribed circle r_{inscrb}. From [10 Eq. 36], the relationship between r_{inscrb} and the length *S* of any side is given by

$$r_{inscrb} = \frac{S}{2\tan(\pi/n)} \tag{43}$$

where *n* is the number of sides in the polygon. Thus, for a regular polygon or circular shaped waveguide, and if reference point *a* in (42) is defined to be at the waveguide centroid, both $x_{i/a_\perp}(\tau)$ and $x_{j/a_\perp}(\tau)$ equate to r_{inscrb}, and (42) with (43) becomes

$$\frac{2\pi}{\lambda_0}\int_{\tau=0}^{\tau=T}\left[x_{i/a_\perp}(\tau)\,\underline{u}_{Inpt_i}(\tau)+x_{j/a_\perp}(\tau)\,\underline{u}_{Inpt_j}(\tau)\right].\underline{\omega}(\tau)\,d\tau$$

$$=\frac{2\pi}{\lambda_0}\int_{\tau=0}^{\tau=T}\left[x_{i/a_\perp}(\tau)+x_{j/a_\perp}(\tau)\right]\omega(\tau)_{Inpt}\,d\tau=\frac{4\pi\,r_{inscrb}}{\lambda_0}\int_{\tau=0}^{\tau=T}\omega(t)_{Inpt}\,dt \qquad (44)$$

$$=\frac{2\pi\,S}{\lambda_0\tan(\pi/n)}\int_{\tau=0}^{\tau=T}\omega(\tau)_{Inpt}\,d\tau$$

Substituting (44) in (41) then obtains for an optical gyro with a regular polygon shaped waveguide:

$$W(T)_m=1+\cos\left[\phi(p,l)-\phi(q,l+\frac{2\pi\,S}{\lambda_0\tan(\pi/n)}\int_{\tau=0}^{\tau=T}\omega(\tau)_{Inpt}\,d\tau\right] \qquad (45)$$

Note, that a circular waveguide of radius r_{crcl} can also be classified as a regular polygon having an infinite number of infinitesimal length sides. Then $n\,S$ is the circumference $2\pi\,r_{crcl}$ of the circle, $\frac{S}{\tan(\pi/n)}\approx\frac{S}{\pi/n}=\frac{n\,S}{\pi}=\frac{2\pi\,r_{crcl}}{\pi}=2\,r_{crcl}$, and substitution in (45) finds

$$W(T)_m=1+\cos\left(\phi(p,l)-\phi(q,l)+\frac{4\pi\,r_{crcl}}{\lambda_0}\int_{\tau=0}^{\tau=T}\omega(\tau)_{Inpt}\,d\tau\right) \qquad (46)$$

A circle of radius r_{inscrb} can also be inscribed in any triangle as given by [10 Eq. 63]:

$$r_{inscrb}=\frac{1}{2}\sqrt{\frac{(b+c-a)(c+a-b)(a+b-c)}{a+b+c}} \qquad (47)$$

where *a*, *b*, and *c* are the lengths of the triangle sides. As for the regular polygon, both $x_{i/a_\perp}$ and $x_{j/a_\perp}$ equate to r_{inscrb}, and the first part of (44) with (47) becomes

$$\frac{2\pi}{\lambda_0}\int_{\tau=0}^{\tau=T}\left[x_{i/a_\perp}(\tau)\,\underline{u}_{Inpt_i}(\tau)+x_{j/a_\perp}(\tau)\,\underline{u}_{Inpt_j}(\tau)\right].\underline{\omega}(\tau)\,d\tau$$

$$=\frac{4\pi\,r_{inscrb}}{\lambda_0}\int_{\tau=0}^{\tau=T}\omega(t)_{Inpt}\,dt=\frac{2\pi}{\lambda_0}\sqrt{\frac{(b+c-a)(c+a-b)(a+b-c)}{a+b+c}}\int_{\tau=0}^{\tau=T}\omega(\tau)_{Inpt}\,d\tau \qquad (48)$$

Substituting (48) in (41) then obtains for a triangular waveguide shaped optical gyro:

$$W(T)_m=1+\cos\left[\phi(p,l)-\phi(q,l)+\frac{2\pi}{\lambda_0}\sqrt{\frac{(b+c-a)(c+a-b)(a+b-c)}{a+b+c}}\int_{\tau=0}^{\tau=T}\omega(\tau)_{Inpt}\,d\tau\right] \qquad (49)$$

NON-PLANAR WAVEGUIDES

Up to this point in the analysis, the only approximation we have made is that (3) is the same as predicted by Relativity theory in (A-1) of the Appendix when v_{ai}^2 is negligibly small compared to c^2, where v_{ai} is the velocity of point *i* relative to point *a* as measured in non-rotating inertial space (i.e., $v_{ai} \equiv \left|\Delta \underline{x}_{i/a} / \Delta t_{i/a}\right|$) and $\Delta t_{i/a}$ is the time interval for the $\Delta \underline{x}_{i/a}$ motion as measured on a point *a* located clock. To derive the equivalent of (45) for optical gyros having non-planar waveguides now requires approximations for $\underline{\omega}(\tau)$ variations during the (41) $\tau = 0$ to $\tau = T$ time interval. Toward this end, first recognize that depending on the optical gyro configuration, the *p*, *q* waves may traverse the closed waveguide once or multiple times. In general then, the integral term in (41) can be divided into successive segments, each representing a single traversal of the waveguide:

$$\begin{aligned} &\int_{\tau=0}^{\tau=T} \left[x_{i/a_\perp}(\tau)\, \underline{u}_{Inpt_i}(\tau) + x_{j/a_\perp}(\tau)\, \underline{u}_{Inpt_j}(\tau) \right] \cdot \underline{\omega}(\tau)\, d\tau \\ &= \sum_k \left\{ \int_{\tau_k=0}^{\tau_k=T_k} \left[x_{i/a_\perp}(\tau_k)\, \underline{u}_{Inpt_i}(\tau_k) + x_{j/a_\perp}(\tau_k)\, \underline{u}_{Inpt_j}(\tau_k) \right] \cdot \underline{\omega}(\tau_k)\, d\tau_k \right\} \end{aligned} \tag{50}$$

where T_k is the time for each *k* wave traversal at the speed of light *c* around the waveguide, and τ_k is the time interval measured on a *k* cycle timer reinitialized to zero for each traversal. Note: To assure that the last *k* cycle will be a complete traversal around the waveguide, the first T_k may only be a partial traversal to match the $\tau_k = 0$ lower limit of the full integrals in (50).

We define the average angular rate over each *k* cycle as

$$\underline{\omega}_{Avg_k} \equiv \frac{1}{T_k} \int_{\tau_k=0}^{\tau_k=T_k} \underline{\omega}(\tau)\, d\tau \tag{51}$$

Approximating angular rate as being constant during each *k* cycle at $\underline{\omega}_{Avg_k}$ sets (50) with (51) to

$$\begin{aligned} &\frac{2\pi}{\lambda_0} \int_{\tau=0}^{\tau=T} \left[x_{i/a_\perp}(\tau)\, \underline{u}_{Inpt_i}(\tau) + x_{j/a_\perp}(\tau)\, \underline{u}_{Inpt_j}(\tau) \right] \cdot \underline{\omega}(\tau)\, d\tau \\ &\approx \frac{2\pi}{\lambda_0} \sum_k \left\langle \left\{ \int_{\tau_k=0}^{\tau_k=T_k} \left[x_{i/a_\perp}(\tau_k)\, \underline{u}_{Inpt_i}(\tau_k) + x_{j/a_\perp}(\tau_k)\, \underline{u}_{Inpt_j}(\tau_k) \right] d\tau_k \right\} \cdot \underline{\omega}_{Avg_k} \right\rangle \end{aligned} \tag{52}$$

Now recognize that the integrals of $x_{i/a_\perp}(\tau_k)\, \underline{u}_{Inpt_i}(\tau_k$ and $x_{j/a_\perp}(\tau_k)\, \underline{u}_{Inpt_j}(\tau_k)$ along the waveguide from $\tau_k = 0$ to $\tau_k = T_k$ will be equal. Thus, (52) simplifies to

$$
\begin{aligned}
&\frac{2\pi}{\lambda_0}\int_{\tau=0}^{\tau=T}\left[x_{i/a\perp}(\tau)\,\underline{u}_{Inpt_i}(\tau)+x_{j/a\perp}(\tau)\,\underline{u}_{Inpt_j}(\tau)\right]\cdot\underline{\omega}(\tau)\,d\tau \\
&\quad\approx\frac{4\pi}{\lambda_0}\sum_k\left\langle\left\{\int_{\tau_k=0}^{\tau_k=T_k}\left[x_{i/a\perp}(\tau_k)\,\underline{u}_{Inpt_i}(\tau_k)\right]d\tau_k\right\}\cdot\underline{\omega}_{Avg_k}\right\rangle \\
&=\frac{4\pi}{\lambda_0}\sum_k\left\langle\left\{\frac{T_k}{cT_k}\int_{\tau_k=0}^{\tau_k=L_k}\left[x_{i/a\perp}(\tau_k)\,\underline{u}_{Inpt_i}(\tau_k)\right]cd\tau_k\right\}\cdot\underline{\omega}_{Avg_k}\right\rangle \\
&=\frac{4\pi}{\lambda_0}\sum_k\left\langle\left\{\frac{1}{L_k}\int_{l_k=0}^{l_k=L_k}\left[x_{i/a\perp}(l_k)\,\underline{u}_{Inpt_i}(l_k)\right]dl_k\right\}\cdot\underline{\omega}_{Avg_k}T_k\right\rangle
\end{aligned}
\tag{53}
$$

where L_k is the total distance around the closed waveguide (and as discussed previously for T_k, may be a partial loop distance for the first *k* cycle), dl_k is the differential distance moved by the *p* wave past point *i* over time interval $d\tau_k$, and l_k is the distance moved by the *p* wave during time interval τ_k.

Lastly we define the average of $x_{i/a\perp}(l_k)\,\underline{u}_{Inpt_i}(l_k)$ in (53) along the closed waveguide as

$$
\left(x_{i/a\perp}\,\underline{u}_{Inpt_i}\right)_{Avg_k}\equiv\frac{1}{L_k}\int_{l_k=0}^{l_k=L_k}\left[x_{i/a\perp}(l_k)\,\underline{u}_{Inpt_i}(l_k)\right]dl_k \tag{54}
$$

Substituting (54) in (53) with (51) and the result into (41), then gives the final form for the non-planar waveguide shaped optical gyro:

$$
\begin{aligned}
W(T)_m&=1+\cos\left[\phi(p,l)-\phi(q,l)+\frac{4\pi}{\lambda_0}\sum_k\ \omega_{InptAvg_k}T_k\right] \\
\omega_{InptAvg_k}&\equiv\left(x_{i/a\perp}\,\underline{u}_{Inpt_i}\right)_{Avg_k}\cdot\underline{\omega}_{Avg_k}
\end{aligned}
\tag{55}
$$

$$
\left(x_{i/a\perp}\,\underline{u}_{Inpt_i}\right)_{Avg_k}\equiv\frac{1}{L_k}\int_{l_k=0}^{l_k=L_k}\left[x_{i/a\perp}(l_k)\,\underline{u}_{Inpt_i}(l_k)\right]dl_k\qquad\underline{\omega}_{Avg_k}\equiv\frac{1}{T_k}\int_{\tau_k=0}^{\tau_k=T_k}\underline{\omega}(\tau)\,d\tau
$$

RING LASER GYROS

A ring laser gyro (RLG) creates two oppositely directed beams of monochromatic light that traverse a closed optical path formed by three or more reflecting mirrors [11; 12]. The beams occupy the same physical space ("optical cavity") and are constrained to travel along a fixed

"waveguide" relative to the gyro by an aperture and curved surface mirror(s). The concept is depicted in Fig. 2 for a 3-mirror RLG configuration, the individual laser beams identified as travelling in the clockwise (cw) and counter-clockwise (ccw) directions.

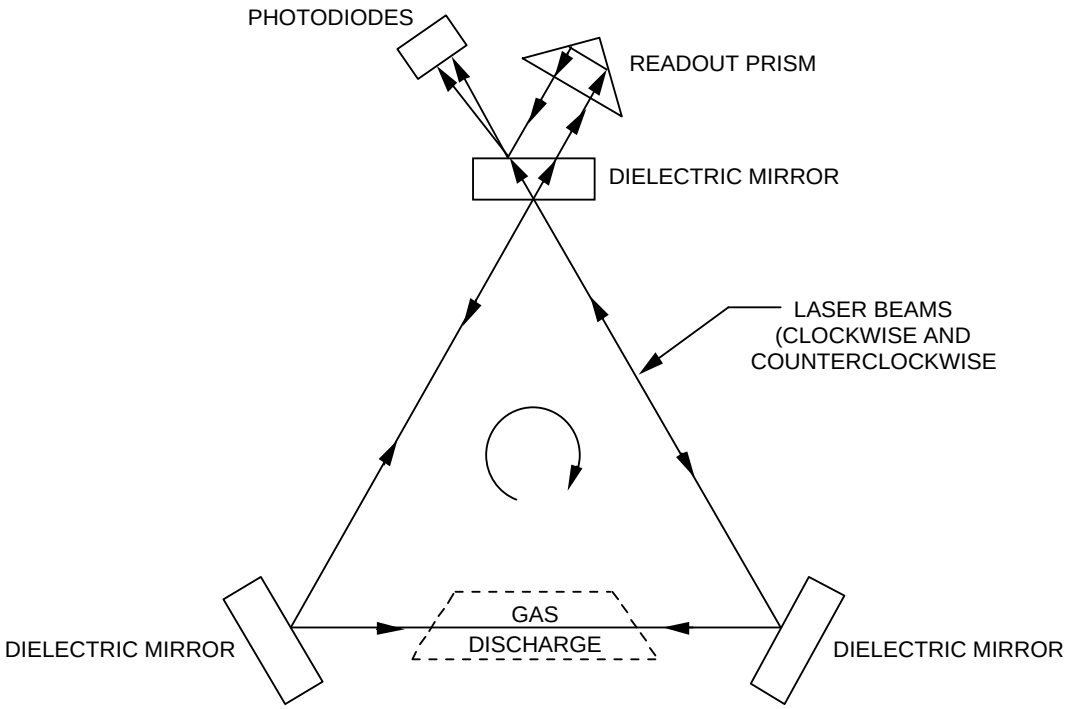

Fig. 2 - Ring Laser Gyro Operating Elements

The RLG light beams in Fig. 2 are sustained by the lasing action of a helium-neon gas discharge within the optical cavity. The reflecting surfaces are dielectric mirrors designed to selectively reflect the frequency associated with the particular helium-neon transition being used (typically of 0.63 micron wavelength). A small fraction of each beam escapes the cavity at the readout, one reflected through a corner prism, then recombined with the other on readout photo detectors. The corner prism is designed to produce a small angle between the recombining beams, thereby creating optical interference fringes on the photo detectors, each illuminated by a different portion of the fringe pattern. The fringe pattern is stationary under zero angular rotation of the cavity. Under cavity rotation, the fringes move across the photo detectors, generating a sinusoidal output at a frequency proportional to the gyro angular rate around its input axis (perpendicular to the plane of the Fig. 2 diagram). Photo detector readout logic converts the sinusoidal output into a digital square wave for each fringe passage. The rise and fall of the square wave edges generate output pulses, each representing an angular rotation through a known angular increment (the gyro output pulse scale factor). Two photo detectors are used, separated from each other by one quarter of a photo-detector-sensed fringe so that resulting sinusoidal outputs are 90 deg phase separated. Comparison between photo detector generated square wave outputs determines the direction of rotation, positive or negative, depending on whether one square wave is leading or lagging the other.

Beam power losses in an RLG are compensated by amplification within the helium/neon plasma, adding photons at the same wavelength and in phase with returning photons (i.e., through Light Amplification by the Stimulated Emission of Radiation – LASER [11; 12]). When lasing is achieved, a returning wave at the same point in the waveguide will be in phase with itself, and the total length of the closed wave path will contain an integral number of wavelengths. To sustain maximum beam power (average of the cw and ccw beams), the wave path is continuously adjusted through path length control (PLC), a closed-loop piezoelectric driven micro-movement of one of the RLG mirrors normal to its surface. Average beam power is measured for the PLC control loop by a separate photo detector mounted on one of the mirror substrates.

The amplification factor ("gain") in a laser is a narrow Gaussian distribution function of light wave frequency (the "atomic gain curve") centered at the nominal wavelength being excited by the Fig. 2 gas discharge (e.g., 0.63 microns for an RLG). An important part of RLG operation is control of the wavelength so that it coincides with the peak of the gain curve. (Operation away from the gain curve peak can produce complex deleterious performance effects that are beyond the scope of this article to explain. For very small RLGs, the impact can be large enough that there is insufficient gain for lasing.) When lasing frequency is at the gain curve peak, beam power is also maximized. Thus, PLC control to maximize beam power implicitly maintains operation at the gain curve peak, thereby stabilizing performance. An added benefit is maximizing illumination of the readout photo detectors, hence, improving output signal-to-noise ratio.

Under zero angular rotation, the RLG He-Ne stimulated emission process provides photons at the clockwise and counterclockwise beam wavelengths, thus assuring that $\lambda_{q/0} = \lambda_{p/0} = \lambda_0$, the basic assumption in (23) leading to general optical gyro combined beam power Eq. (41) for RLG application. Under non-zero angular rotation, "Doppler broadening" within the He-Ne transition process [12] provides the mechanism for adding in-phase photons to returning *p*, *q* waves at their (23) shifted $\lambda_{p/i}$, $\lambda_{q/j}$ wavelengths embedded in (41).

RLG Analytical Model

The RLG He-Ne transition process generates new *p* and *q* oppositely travelling photons at the same phase and frequency as returning photons. This creates the illusion that each photon is repeatedly traversing the wave path. The result can be analytically represented by (41), a combined beam power input to the RLG photo detectors representing the integral of angular rate from the first time since laser ignition (at running time $\tau = 0$) that the cw and ccw waves simultaneously appear in the waveguide in the point *l* "readout zone" (where the photo diode readout detectors are located in Fg. 2). In (41), $\phi(p,l) - \phi(q,l)$ represents the difference in phase between the Fig. 2 cw and ccw light beams at $\tau = 0$, and running time $\tau = T$ represents the current time in the readout zone (at point *m*, the same as point *l*, but at a later time).

A fundamental distinction between an RLG and a FOG (to be described subsequently) is that in a FOG, $\tau = 0$ represents a "computer controlled" time instant when an integrated angular rate output increment measurement begins, current time $\tau = T$ represents the time the output

measurement is made, and $\tau = T$ also represents the time instant when the next angular incremental measurement begins. Sequential non-overlapping incremental measurements follow, each of duration *T*, the time for a wave front to travel along the fiber optic wave path from the input light emitting diode source to the output photo detector.

In contrast, for an RLG, $\tau = 0$ represents the first time since laser ignition that the light beam wave fronts (cw and ccw) appear simultaneously in the readout zone, while $\tau = T$ represents any time since $\tau = 0$ that the laser beams are combining continuously in the readout zone. To distinguish this difference, we will equate *T* to any general time interval *t* since $\tau = 0$ so that (41) becomes the revised form

$$W(t)_m = 1 + \cos\left\{\phi_{l/p_0} - \phi_{l/q_0} + \frac{2\pi}{\lambda_0}\int_{\tau=0}^{\tau=t}\left[x_{i/a_\perp}(\tau)\,\underline{u}_{Inpt_i}(\tau) + x_{j/a_\perp}(\tau)\,\underline{u}_{Inpt_j}(\tau)\right].\underline{\omega}(\tau)\,d\tau\right\} \quad (56)$$

The effect of (56) is to generate an optical interference pattern ("fringes") across the readout zone photo diodes (Fig. 2). This can be analytically represented by first defining another point m' located in the readout zone, displaced from *m* by a small distance *s* "ahead" of *m* in the cw beam direction. At arbitrary time *t*, the phase $\phi(t)_{p/m'}$ of the clockwise *p* beam at point m' will equal the phase $\phi(t)_{p/m}$ at *m* plus small distance Δs from *m* to m' (measured in 2π wavelengths), i.e., $\phi(t)_{p/m'} = \phi(t)_{p/m} + \frac{2\pi}{\lambda_m}\Delta s$ where λ_m is the cw light beam wavelength at point *m*. Similarly, the phase of the ccw *q* beam (travelling in the opposite direction) will be reduced by the same amount: $\phi(t)_{q/m'} = \phi(t)_{q/m} - \frac{2\pi}{\lambda_m}\Delta s$. Then, incorporating the $T \equiv t$ generalization, the equivalent to (35) for point m' will be

$$\begin{aligned}
\phi(t)_{p/m'} &= \phi(p,l) + \frac{2\pi}{\lambda_m}\Delta s + \frac{2\pi}{\lambda_0}\left[ct + \int_{t=0}^{\tau=t} x_{i/a_\perp}(\tau)\,\underline{u}_{Inpt_i}(\tau)\,.\,\underline{\omega}(\tau)\,d\tau\right] \\
\phi(t)_{q/m'} &= \phi(q,l) - \frac{2\pi}{\lambda_m}\Delta s + \frac{2\pi}{\lambda_0}\left[ct - \int_{t=0}^{\tau=t} x_{i/a_\perp}(\tau)\,\underline{u}_{Inpt_i}(\tau)\,.\,\underline{\omega}(\tau)\,d\tau\right]
\end{aligned} \quad (57)$$

Eqs. (57) shows that the Δs displacement creates the equivalent of a shift in the initial phase of the laser beams by $\frac{2\pi}{\lambda_m}\Delta s$, positive for the cw beam, and negative for the ccw beam. The result is the revised equivalent of the (56) combined beam power equation for point m':

$$W(t)_{m'} = 1 + \cos\left\{\begin{array}{c}\phi_{l/p_0} - \phi_{l/q_0} + 2\pi\dfrac{\Delta s}{\lambda_m/2} \\ +\dfrac{2\pi}{\lambda_0}\displaystyle\int_{\tau=0}^{\tau=t}\left[x_{i/a_\perp}(\tau)\,\underline{u}_{Inpt_i}(\tau) + x_{j/a_\perp}(\tau)\,\underline{u}_{Inpt_j}(\tau)\right].\underline{\omega}(\tau)\,d\tau\end{array}\right\} \quad (58)$$

Eq. (58) shows that at any general time *t*, the beam power $W(t)_{m'}$ will repeat cyclically with location Δs across the readout zone as the cosine of 2π times the fraction of Δs over half the local light beam wavelength λ_m. This is an analytical representation of the optical interference "fringes" (light and dark bands) generated across the readout zone by the combined energy in the cw and ccw laser beams.

More importantly, for an RLG, (56) and (58) also shows that the fringes will translate across the readout zone by the integral of angular rate $\underline{\omega}(\tau)$ as time *t* progresses into the future, repeating itself in time each time the $\underline{\omega}(\tau)$ weighted integral generates a specific integrated angular rate increment, i.e., when $\frac{1}{\lambda_0}\int_{\tau=t}^{\tau=t+\Delta t}\left[x_{i/a_\perp}(\tau)\,\underline{u}_{Inpt_i}(\tau)+x_{j/a_\perp}(\tau)\,\underline{u}_{Inpt_j}(\tau)\right].\underline{\omega}(\tau)\,d\tau=1$, where Δt is the time increment when the previous equality is true. Thus, for an optical photodiode pickoff located in the readout zone, angular rotation will generate a sinusoidal cyclic output, repeating each time the integrated angular rate accumulates that specific integrated angular rate increment (the fundamental measurement "pulse size").

Counting the output cycles would digitally measure the integrated angular rate around the gyro input axis. The output digitization process is implemented by first converting the analog sinusoidal pickoff output signal to an equivalent square wave, each change (minus to plus or plus to minus) indicating a gyro angular rotation of half the fundamental pulse size. The sign (plus or minus) of the rotation measurement is determined by adding a second photodiode at point m' in the readout zone, displaced from the one a point *m* by linear distance Δs to generate a phase shift from the *m* photodiode by 90 deg ($\pi/2$). The length of Δs is analytically found from (58) by specifying $2\pi\frac{\Delta s}{\lambda_m/2}=\pi/2$ which finds $\Delta s=\lambda_m/8$.

Generating a square wave from the m' diode creates a square wave that is 90 deg phase shifted from the *m* diode created square wave, the m' "states" (plus or minus) overlapping the state changes from the *m* square wave. Digital logic assigns a plus to the *m* sensed rotation when the *m* square wave state change finds a plus state on the m' square wave. Conversely, the rotation is negative when the *m* state change is accompanied by a negative m' state. Once the *m* and m' square wave measurements are implemented, the capability then exists to generate outputs not only for the *m* square wave state changes, but also for the m' square wave state changes. The method duplicates what was described for the *m* wave measurements, with the m' wave state change now used to indicate the rotation occurrence. Thus, 4 rotation occurrence outputs would be generated for each cycle of the photodiode outputs, 2 from the *m* wave, 2 from the m' wave, all spaced one quarter of a wavelength apart, the equivalent of reducing the output "pulse size" by a factor of 4.

Eq. (56) or (58) can also be used to assess the RLG output scale factor for a particular waveguide geometry; triangle, regular polygon, or general out-of-plane shape as in (45), (49), and (55) for the point *m* photo detector. For example, for a regular polygon, (45) (with $T\equiv t$) shows that the normalized power at a point *m* located photo detector will cyclically repeat each

time $\frac{2\pi S}{\lambda_0 \tan(\pi/n)} \int_{\tau=0}^{\tau=t} \omega(\tau)_{Inpt}\, d\tau$ changes by 1, corresponding to an output "scale factor" of $1/\left[\frac{S}{\lambda_0 \tan(\pi/n)}\right]$ radians change in integrated angular change input $\int_{\tau=0}^{\tau=t} \omega(\tau)_{Inpt}\, d\tau$ per photo detector output cycle. For an equilateral triangular RLG (i.e., $n = 3$) with $S = 4.2$ inches per side (0.35 ft) and the commonly used visible RLG wavelength λ_0 of 0.63 micron (2.02 e-6 ft), the photo detector output scale factor will be

$$1/\left[\frac{S}{\lambda_0 \tan(\pi/n)}\right] = 1/\left(\frac{0.35}{2.02e-6 \times 1.732}\right) = 1.00\, e-5 \text{ radians} = 2.06 \text{ arc sec per output cycle}.$$

By triggering two output pulses (one at each photo detector output half cycle) from each of the two photo detectors (being position phased in "quadrature" - 90 degrees apart as described previously), the combined output pulse scale factor would be 2.06 / 4 = 0.515 arc sec per pulse.

A square RLG configuration would have $n = 4$. For a scale factor equivalent to the previously described 4.2 inch per side triangular RLG, the square RLG would have

$$1/\left[\frac{S}{\lambda_0 \tan(\pi/n)}\right] = 1/\left(\frac{S}{2.02\ e-6 \times 1.00}\right) = \frac{2.02e-6}{S} = 1.00\, e-5 \text{ for which}$$

$S = 0.202$ ft = 2.42 inches = 6.15 centimeters, corresponding to a perimeter of 24.6 centimeters.

FIBER-OPTIC GYROS

A fiber optic gyro (FOG) consists of a circular coil of optical fiber, the ends optically spliced together with fiber-optic couplers that route near monochromatic light from a super-luminescent diode (e.g., gallium arsenide) into and out of the coil [13 pp 186-190; 14; 15]. The concept is depicted in Fig. 3.

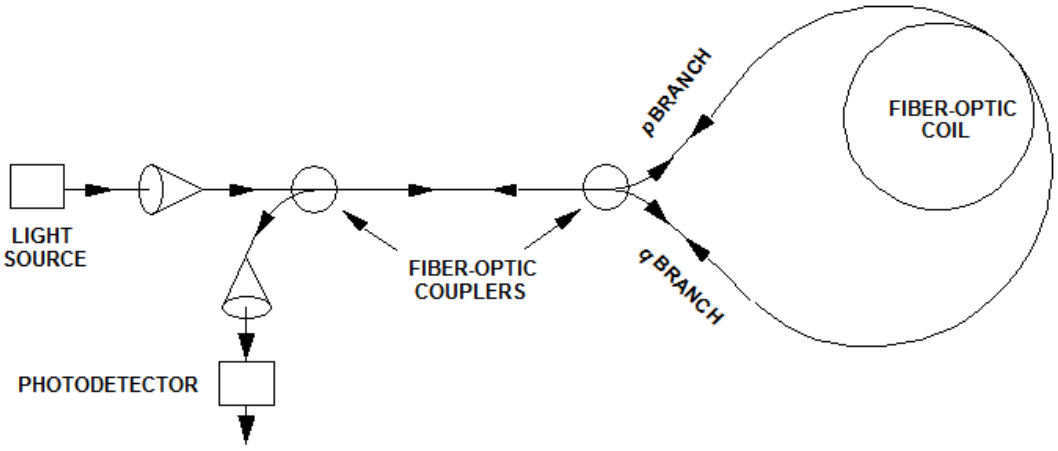

Fig. 3 - Fiber Optic Gyro (FOG) Concept

The light beam from the photo diode light source in Fig. 3 passes through a first coupler, then into the fiber-coil through a second coupler where it splits into two beams, one into the *p* branch, the other oppositely directed into the *q* branch. After traversing the coil, the beams recombine in the second coupler, and are gated through the first coupler to a readout photo detector. Under rotation, the *p* and *q* branch beams experience a relative phase shift, generating a change in the combined beam power illuminating the photo detector. Readout electronics convert the photo detector output into a measurement of angular rotation that created the phase shift.

Fundamental FOG Analytical Model

As with the RLG, the fundamental operation of a FOG can be represented by (41), describing the continuous light wave emitted from the diode light source in Fig. 3. The basic difference in fiber optic and ring laser gyro operation is that for a FOG, each light beam wave front traverses the waveguide once for sampling from its closed optical path entry at the photo-diode light source to the pickoff. In contrast, light waves in an RLG traverse the waveguide continually (being continuously reinforced in phase and wavelength by the He-Ne stimulated emission process). Thus, in an RLG, the $\tau = 0$ to $\tau = t$ time interval (where $T \equiv t$ in (41) represents the current time since laser ignition whereas in a FOG, $\tau = 0$ to $\tau = T$ represents the time interval for a wave front to reach the pickoff after once traversing the optical fiber beam path. Since the counter-travelling photons in a FOG originate from the same monochromatic light source, they have the same wavelength under zero angular change, hence, $\lambda_{0_q} = \lambda_{0_p} = \lambda_0$ in (23), the effect embedded in (41). Additionally, since the counter-travelling photons enter the waveguide at the same phase, $\phi(p,l) - \phi(q,l)$ in (41) is zero. Thus, for the Fig. 3 FOG configuration, the general (41) analytical power model simplifies to

$$W(T)_m = 1 + \cos\left\{\frac{2\pi}{\lambda_0}\int_{\tau=0}^{\tau=T}\left[x_{i/a_\perp}(\tau)\,\underline{u}_{Inpt_i}(\tau) + x_{j/a_\perp}(\tau)\,\underline{u}_{Inpt_j}(\tau)\right].\underline{\omega}(\tau)\,d\tau\right\} \qquad (59)$$

where *T* is the time interval for a photon to traverse the fiber coil from the light source to the pickoff.

The optical fiber winding process for a FOG generates a waveguide configuration that is inherently non-planar (but approximately planar). Eq. (55) with $\phi(p,l) - \phi(q,l)$ equal to zero describes the equivalent non-planar FOG version of (59):

$$W(T)_m = 1 + \cos\left(\frac{4\pi}{\lambda_0}\sum_k \omega_{InptAvg_k} T_k\right)$$

$$\omega_{InptAvg_k} \equiv \left(x_{i/a_\perp}\,\underline{u}_{Inpt_i}\right)_{Avg_k} \cdot \underline{\omega}_{Avg_k} \qquad (60)$$

$$\left(x_{i/a_\perp}\,\underline{u}_{Inpt_i}\right)_{Avg_k} \equiv \frac{1}{L_k}\int_{l_k=0}^{l_k=L_k}\left[x_{i/a_\perp}(l_k)\,\underline{u}_{Inpt_i}(l_k)\right]dl_k \qquad \underline{\omega}_{Avg_k} \equiv \frac{1}{T_k}\int_{\tau_k=0}^{\tau_k=T_k}\underline{\omega}(\tau)\,d\tau$$

For a fiber length of 1000 meters, the time for a photon to traverse the fiber coil at the speed of light (3 e8 meters/sec) would be T = 1000 / 3 e8 = 3.33 e-6 sec.

If the fiber coil is approximated as a connected set of n parallel overlapping circular segments, the discussion preceding and following (46) shows that $x_{i/a\perp}$ in (60) equals r_{crcl}, the radius of each circular segment, and $\underline{u}_{Inpt_i}$ is the gyro input unit vector $\underline{u}_{Inpt}$ perpendicular to the plane of the concentric circles (i.e., $x_{i/a\perp}\,\underline{u}_{Inpt_i} = r_{crcl}\,\underline{u}_{Inpt}$). Thus, for a FOG, (60) approximates as

$$\begin{aligned}
\omega_{InptAvg_k} &\equiv \left(x_{i/a\perp}\,\underline{u}_{Inpt_i}\right)_{Avg_k} \cdot \underline{\omega}_{Avg_k} = \frac{r_{crcl}}{T_k}\,\underline{u}_{Inpt} \cdot \int_{\tau_k=0}^{\tau_k=T_k} \underline{\omega}(\tau)\,d\tau \\
&= \frac{r_{crcl}}{T_k} \int_{\tau_k=0}^{\tau_k=T_k} \underline{u}_{Inpt} \cdot\, \underline{\omega}(\tau)\,d\tau = \frac{r_{crcl}}{T_k} \int_{\tau_k=0}^{\tau_k=T_k} \omega_{Inpt}\,d\tau \\
W(T)_m &= 1+\cos\left(\frac{4\pi}{\lambda_0}\sum_k\ \omega_{InptAvg_k} T_k\right) = 1+\cos\left[\frac{4\pi}{\lambda_0}\sum_k\ \frac{r_{crcl}}{T_k}\left(\int_{\tau_k=0}^{\tau_k=T_k} \omega_{Inpt}\,d\tau\right)T_k\right] \\
&= 1+\cos\left(\frac{4\pi\, r_{crcl}}{\lambda_0} \int_{\tau=0}^{\tau=T} \omega_{Inpt}\,d\tau\right)
\end{aligned} \tag{61}$$

or equivalently,

$$W(T)_m = 1+\cos\left(\frac{4\pi\, r_{crcl}}{\lambda_0}\,\Delta\theta_{Inpt}(T)\right) \qquad \Delta\theta_{Inpt}(T) \equiv \int_{\tau=0}^{\tau=T} \omega_{Inpt}\,d\tau \tag{62}$$

where $W(T)_m$ is the output signal from the FOG photodiode output detector at point m (the end of the fiber coil) at time interval T, the time for a wave front to traverse the fiber coil at the speed of light (over fiber coil length L) from the FOG light emitting diode at point l (at the start of the fiber coil) to the optical pickoff at point m (at the end of the fiber coil), r_{crcl} is the radius of each circular element in the fiber coil, and $\Delta\theta_{Inpt}(T)$ is the integral over time period T of the angular rate component along the FOG input axis $\underline{u}_{Inpt}$ (perpendicular to the fiber coil plane). If each circular segment has a 3 inch diameter (1.5 inch radius) and the light source wavelength λ_0 is 0.82 microns (typical for a FOG gallium-arsenide photo-diode light source), under an average angular rate ω_{Inpt} of 7 rad/sec (approximately 400 deg/sec), the bracketed phase angle in (62) induced at the FOG pickoff would be

$$\frac{4\pi\, r_{crcl}}{\lambda_0}\,\Delta\theta_{Inpt}(T) = \frac{4\pi}{0.82e-6}\times 1.5\times 0.0254\times 7\times 3.33e-6 = 13.6 \text{ rad}.$$

To be useful for computing angular orientation in system applications, it is important that the FOG output $W(T)_m$ measurements of $\Delta\theta_{Inpt}(T)$ in (62) represent successive increments of

angular change (for each successive T interval). Then, using simultaneous outputs from three orthogonally mounted FOGs, they can be used effectively in an appropriate algorithm for repetitive three-dimensional attitude computation updating. Since each measurement of $W(T)_m$ in (62) represents an attitude change $\Delta\theta_{Inpt}(T)$ over T, this means that the $W(T)_m$ measurements must be sampled and output at a frequency of $1 / T$. For T = 3.33 e-6 sec in the previous example, this translates into a $W(T)_m$ measurement/sampling rate of 1 / 3.33 e-6 = 0.3 mega-Hz.

"Closed-Loop" FOG Configuration

A significant difference between the RLG and FOG arises in the complexity of the readout implementation. Most high accuracy mechanical gyros have been implemented in the past using narrow angle pickoffs designed to operate over a small angular input range (e.g., 1 milli-rad). The purpose is to minimize the effect of pickoff scale factor error on device performance. It is typically achieved by controlling the pickoff output in servo feedback fashion to dynamically maintain the pickoff output (hence, pickoff input) at zero (null). This has been achieved by either mechanically controlling the base to which the gyro is mounted (i.e., with a mechanical gimbaled platform), or by using electrical "closed-loop" rebalance whereby an electrical signal is generated from the pickoff output to provide angular rate bias feedback within the gyro to maintain pickoff null [16]. A closed-loop gyro output would then be generated within the rebalance loop from the biasing signal required to maintain pickoff null, thereby becoming equal but opposite to the gyro dynamic angular input.

Eq. (62) illustrates the fundamental difficulty of measuring the scaled angular increment $\Delta\theta_{Inpt}(T)$ with an "open-loop" FOG; the lack of sensitivity in power $W(T)_m$ for small $\Delta\theta_{Inpt}(T)$, the inverse cosine function in $W(T)_m - 1$ becoming indeterminate at zero $\Delta\theta_{Inpt}(T)$, and prone to significant scale factor error (from pickoff output non-linearity characteristics) at non-zero angular increments. For a closed-loop FOG, the goal is to create closed-loop electrical bias that maintains $W(T)_m$ at a known value with high sensitivity for any value of $\Delta\theta_{Inpt}(T)$. Thus, means must be introduced to enable measuring deviations from a specified $W(T)_m$ beam power, and providing "closed loop" feedback to maintain $W(T)_m$ at its specified value under all dynamic angular rate conditions.

For a closed–loop FOG, the equivalent to (62) also derives from (55), but having $\phi(p,l)$ and $\phi(q,l)$ include additional bias introduced within the fiber coil to enable closed-loop operation and $\Delta\theta_{Inpt}(T)$ determination under any input condition. Thus in (55), $\phi(p,l) = \alpha + \Delta\beta_p$ and $\phi(q,l) = \alpha + \Delta\beta_q$ where α is the phase of the light beam entering the coil (splitting into p and q branches as in Fig. 3), and $\Delta\beta_p$, $\Delta\beta_q$ represent additional phase biases intentionally introduced in the p, q branches within the coil. The closed-loop equivalent to (62) then derives from (55) using the same rationale that led to (62):

$$
\begin{aligned}
W(T)_m &= 1+\cos\left[\phi(p,l)-\phi(q,l)+\frac{4\pi}{\lambda_0}\sum_k \omega_{InptAvg_k}T_k\right] \\
&= 1+\cos\left[\left(\alpha+\Delta\beta_p\right)-\left(\alpha+\Delta\beta_q\right)+\frac{4\pi}{\lambda_0}\sum_k \omega_{InptAvg_k}T_k\right] \\
&= 1+\cos\left(\Delta\beta_p-\Delta\beta_q+\frac{4\pi}{\lambda_0}\sum_k \omega_{InptAvg_k}T_k\right)
\end{aligned}
\tag{63}
$$

with $\omega_{InptAvg_k}$ as defined in (61). Then, using the approximation that the fiber coils are circular and parallel, the analysis leading to (62) has (63) becoming with condensed notation

$$
\begin{aligned}
W(T)_m &= 1+\cos\left[\Delta\phi+\left(\Delta\beta_p-\Delta\beta_q\right)\right] \qquad \Delta\phi \equiv k_{SF}\,\Delta\theta_{Inpt}(T) \\
k_{SF} &\equiv \frac{4\pi}{\lambda_0}\,r_{crcl} \qquad \Delta\theta_{Inpt}(T) \equiv \int_{\tau=0}^{\tau=T} \omega_{Inpt}\,d\tau
\end{aligned}
\tag{64}
$$

where λ_0 is the nominal wavelength of the FOG laser light (at zero input rate), r_{crcl} is the radius of each fiber coil, T is the total time for a FOG light wave front to traverse the fiber coil from the beginning (at coil entry point l) to the end (at coil exit point m), and $\Delta\theta_{Inpt}(T)$ is the integrated angular rate ω_{Inpt} over T along the FOG input axis (perpendicular to the fiber coil plane). The FOG scale factor k_{SF} in (64) shows that there will be a $\frac{4\pi r_{crcl}}{\lambda_0}$ shift in phase $\Delta\phi$ between light waves reaching the readout photo detector per radian of inertial angular rotation $\Delta\theta_{Inpt}(T)$ during time interval T for a light beam wave front to traverse the fiber coil. For comparison, (46) applied to a hypothetical RLG with circular shaped waveguide of radius r_{crcl} shows that there would be a $\frac{4\pi}{\lambda_0}\,r_{crcl}$ phase shift between light waves reaching the readout per radian angular change $\Delta\theta_{Inpt}(T)$ in inertial angular rotation. Thus, both the FOG and RLG measure angular rotation changes by the same scale factor.

In modern day FOGs, integrated optics inserts are used to generate the $\Delta\beta_p$ and $\Delta\beta_q$ applied phase shifts in (64), based on the use of active electro-optic crystals that change the index of refraction of light passing through. With this approach, the integrated optics insert is constructed from a crystal of lithium-niobate using titanium strips diffused on the surface to gate light waves through the crystal [13 pp 189-190]. Voltage applied across the crystal changes the index of refraction of light passing through, changing the speed of light waves propagating through the crystal, thereby adding phase shift.

For a given applied voltage, the same phase shift will be added to waves entering from either side of the crystal, i.e., from the p or q wave directions in a FOG fiber coil. Achieving a net

phase difference in (64) relies on the crystal being inserted at one end of the fiber to take advantage of the time interval difference for a *p* wave (for example) to reach the readout photo detector compared to the *q* wave. Thus, imagine a crystal inserted at the end of the coil where the *p* wave begins its journey. Then a voltage V_1 (corresponding to a β_1 phase shift) applied to the crystal at current time t_1 will shift the *p* wave phase by $\Delta\beta_p = \beta_1$, but this shift will not appear on the photo detector until *p* completes its passage around the coil at a later time t_2. Now consider a *q* wave that entered the coil with *p* at time t_1, but travelling in the opposite direction from *p* around the coil, did not pass through the crystal until time t_2. If V_2 is being applied to the crystal at time t_2 (with corresponding phase shift β_2), the *q* wave will be phase shifted by $\Delta\beta_q = \beta_2$ when it reaches the photo detector at t_2. The net result is that at time t_2, the *p* and *q* waves with phase shifts $\Delta\beta_p$ and $\Delta\beta_q$ will combine on the photo detector to generate a phase shift difference $\Delta\beta_p - \Delta\beta_q = \beta_1 - \beta_2$ in the (64) beam power, depending on the logic used in setting V_1 and V_2. An example of applying this concept is depicted in Fig. 4, a closed-loop FOG version of Fig. 3.

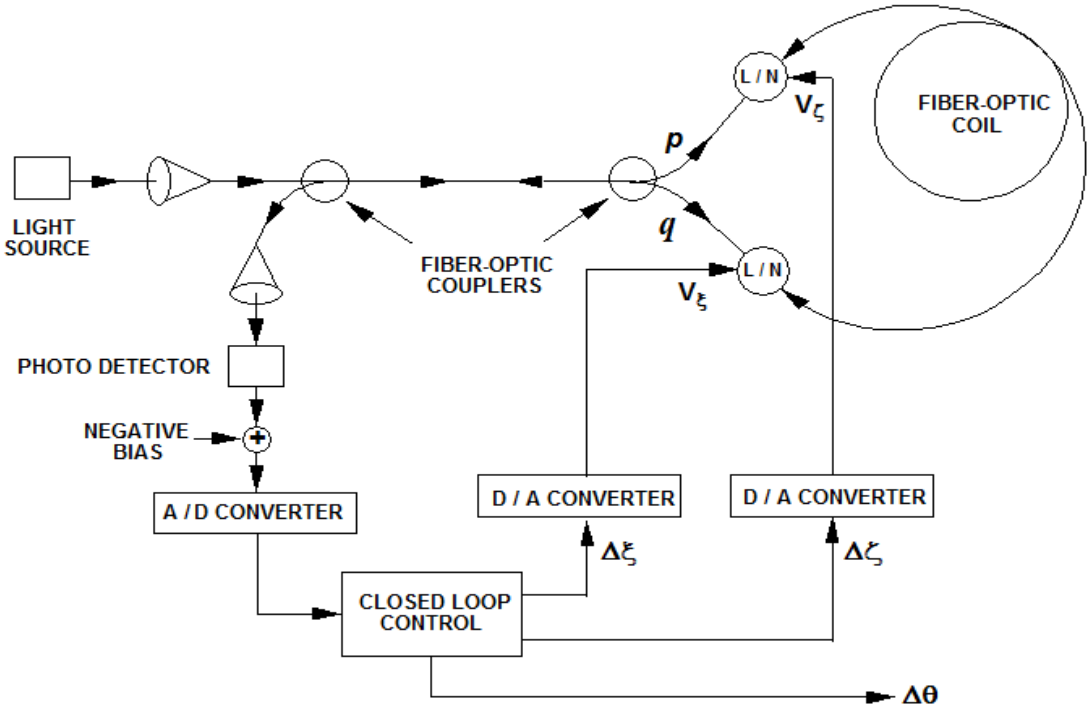

Fig. 4 – Closed-Loop FOG Configuration

A general goal in the design of inertial components is to provide symmetry to minimize the likelihood of asymmetric anomalous error generation. For a FOG, a symmetric design approach would use two lithium-niobate (L/N) crystals symmetrically placed in the *p* and *q* photon light paths at equal distances from the fiber coil junction, one located in the *p* branch, the other in the *q* branch. The symmetric configuration in Fig. 4 shows how the photo detector output would then be applied in feedback fashion through the Closed Loop Control computation block to

generate $\Delta\varsigma$, $\Delta\xi$ phase shifts in the *p*, *q* waves through V_ς, V_ξ voltages applied to the two L/N crystals. (The analog Negative Bias signal applied to the Analog-to-Digital (A/D) Converter input in Fig. 4 will be discussed later.) In conjunction with generating the $\Delta\varsigma$, $\Delta\xi$ phase shift commands, Closed Loop Control in Fig. 4 also computes $\Delta\theta_{Inpt}(T)$ angular increment measurements for output.

From (64) at time t_i, the combined *p* and *q* beam power illuminating the photo detector in Fig. 4 would be $W_i = 1 + \cos\left[\Delta\phi_i + \left(\Delta\beta_{p_i} - \Delta\beta_{q_i}\right)\right]$. The $\Delta\beta_{p_i}$ and $\Delta\beta_{q_i}$ phase shifts induced in W_i as a function of the applied $\Delta\varsigma$, $\Delta\xi$ commands can be determined from Fig. 5 by following the progress of the *p* and *q* waves as they enter and leave the fiber coil.

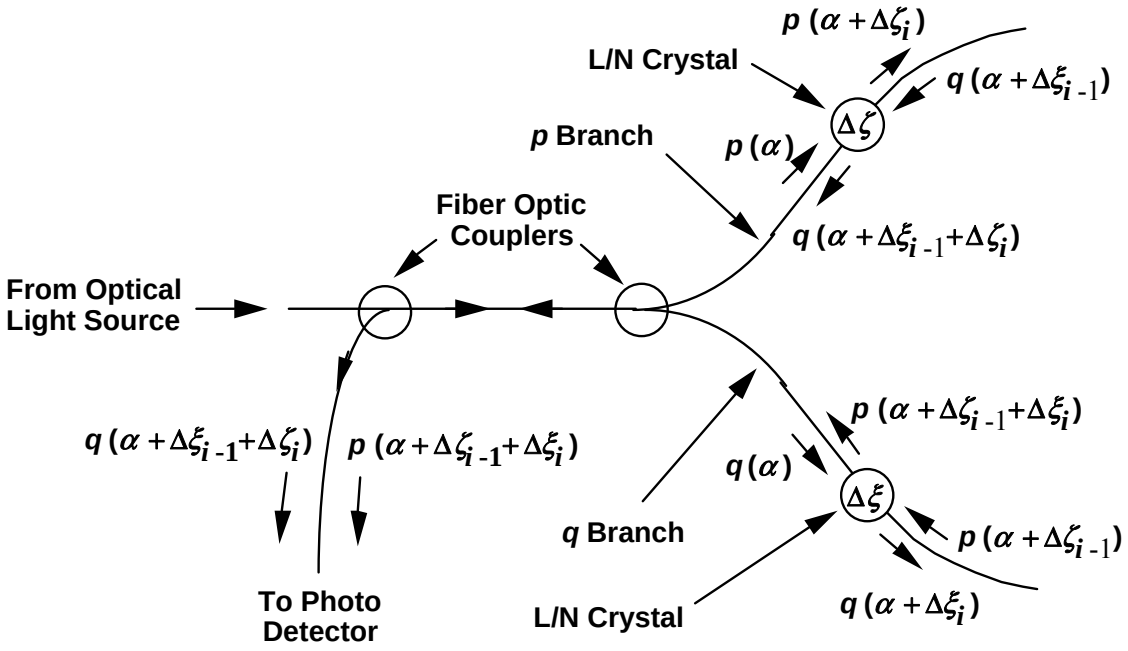

Fig. 5 – Closed-Loop FOG Signal Flow

At time t_i, a light wave at phase α from the Optical Light Source passes through the first coupler in Fig. 5, is gated into the fiber coil by the second coupler, then splits into *p* and *q* branches, each with phase α as denoted by $p(\alpha)$ and $q(\alpha)$. The *p* branch crystal imparts $\Delta\varsigma_i$ additional phase to the *p* wave at time t_i, generating $\alpha + \Delta\varsigma_i$ phase on the *p* output, denoted in Fig. 5 as $p(\alpha + \Delta\varsigma_i)$. Simultaneously at time t_i, a returning *q* wave at $q(\alpha + \Delta\xi_{i-1})$ (i.e., previously phase shifted by $\Delta\xi_{i-1}$ at t_{i-1} by the *q* branch crystal) enters the *p* branch crystal, leaves at $q(\alpha + \Delta\xi_{i-1} + \Delta\varsigma_i)$, and is gated by the coupler to the readout Photo Detector. Thus, $\Delta\beta_{q_i}$ in (64), the shift in *q* wave phase from its α value at coil entry, will be $\Delta\beta_{q_i} = \Delta\xi_{i-1} + \Delta\varsigma_i$.

Similarly, the *q* branch crystal will impart $\Delta\xi_i$ additional phase to the *q* wave at time t_i, generating $q(\alpha+\Delta\xi_i)$ for the *q* output in Fig. 5. Simultaneously at time t_i, a returning *p* wave at $p(\alpha+\Delta\varsigma_{i-1})$ enters the *q* branch crystal, leaves at $p(\alpha+\Delta\varsigma_{i-1}+\Delta\xi_i)$, and is gated by the coupler to the readout photo detector. Thus, $\Delta\beta_{p_i}$ in (64), the shift in *p* wave phase from its α value at coil entry, will be $\Delta\beta_{p_i}=\Delta\varsigma_{i-1}+\Delta\xi_i$.

The net result is that at time t_i, the *p* and *q* waves will recombine as in (64) to have a total beam power input to the Fig. 5 photo detector of

$$\begin{aligned} W_i &= 1+\cos\left[\Delta\phi_i+\left(\Delta\beta_{p_i}-\Delta\beta_{q_i}\right)\right]=1+\cos\left\{\Delta\phi_i+\left[\left(\Delta\varsigma_{i-1}+\Delta\xi_i\right)-\left(\Delta\xi_{i-1}+\Delta\varsigma_i\right)\right]\right\} \\ &= 1+\cos\left[\Delta\phi_i-\left(\Delta\varsigma_i-\Delta\varsigma_{i-1}\right)+\left(\Delta\xi_i-\Delta\xi_{i-1}\right)\right] \end{aligned} \tag{65}$$

The W_i photo detector measurement of (65) would be saved by the Fig. 4 Closed Loop Control at time t_i. The $\Delta\varsigma_{i-1}$ and $\Delta\xi_{i-1}$ values in (65) would have been previously set during the time interval between t_{i-2} to t_{i-1}, thus, generating the equivalent of (65) at time t_{i-1} of

$$W_{i-1}=1+\cos\left[\Delta\phi_{i-1}-\left(\Delta\varsigma_{i-1}-\Delta\varsigma_{i-2}\right)+\left(\Delta\xi_{i-1}-\Delta\xi_{i-2}\right)\right] \tag{66}$$

The W_{i-1} photo detector measurement of (66) would have been saved in the Fig. 4 Closed Loop Control block at time t_{i-1}.

Between times t_i and t_{i+1}, the W_i readout from (65) (stored at time t_i) would be combined with W_{i-1} from (66) (stored at time t_{i-1}) to calculate $\Delta\phi_i$ for output (between t_i and t_{i+1}) and to maintain closed-loop control. The closed-loop control method selected depends on the analytical approach used in setting the $\Delta\varsigma$ s and $\Delta\xi$ s in (65) and (66). Examples are described next.

Examples of Closed-Loop FOG Control

Consider having the cosine function in (65) controlled to zero. Then the corresponding control law would be

$$\left(\Delta\varsigma_i-\Delta\varsigma_{i-1}\right)-\left(\Delta\xi_i-\Delta\xi_{i-1}\right)=\widehat{\Delta\phi_i}\pm\pi/2+2\,n_i\,\pi \tag{67}$$

where $\widehat{\Delta\phi_i}$ is the control loop estimate for $\Delta\phi_i$ in (65) and n_i is an arbitrary integer (to be subsequently chosen based on other considerations). With (67), and assuming that closed-loop operations maintain $\widehat{\Delta\phi_i}\approx\Delta\phi_i$, (65) becomes for cycle *i* :

$$W_i = 1 + \cos\left[\Delta\phi_i - \left(\Delta\varsigma_i - \Delta\varsigma_{i-1}\right) + \left(\Delta\xi_i - \Delta\xi_{i-1}\right)\right]$$
$$= 1 + \cos\left(\Delta\phi_i - \widehat{\Delta\phi_i} \mp \pi/2 - 2\,n_i\,\pi\right) = 1 \pm \sin\left(\Delta\phi_i - \widehat{\Delta\phi_i}\right) \tag{68}$$

In principle, (68) can be used to calculate $\Delta\phi_i$ using $\Delta\phi_i = \widehat{\Delta\phi_i} \mp \sin^{-1}(W_i - 1)$. This could be implemented for example, by applying the minus "1" as the Negative Bias signal in Fig. 4 to the photo detector output before sampling by the D/A converter. The problem with this approach is that the "1" in (68) assumes accurate knowledge of normalizing scale factor B^2 in the (39) definition of normalized power W. To eliminate this error source, the minus option for the $\mp$ polarity in (68) is used for the W_i measurement, and the plus option for the previous W_{i-1} measurement. Then, similar to the (68) derivation from (66), the W_{i-1} and W_i measurements would become:

$$W_{i-1} = 1 + \cos\left[\Delta\phi_{i-1} - \left(\Delta\varsigma_{i-1} - \Delta\varsigma_{i-2}\right) + \left(\Delta\xi_{i-1} - \Delta\xi_{i-2}\right)\right]$$
$$= 1 + \cos\left(\Delta\phi_{i-1} - \widehat{\Delta\phi_{i-1}} + \pi/2 - 2\,n_{i-1}\,\pi\right) = 1 - \sin\left(\Delta\phi_{i-1} - \widehat{\Delta\phi_{i-1}}\right)$$
$$= 1 - \left(\Delta\phi_{i-1} - \widehat{\Delta\phi_{i-1}}\right) + \left(\Delta\phi_{i-1} - \widehat{\Delta\phi_{i-1}}\right)^3/6 + \cdots$$
$$W_i = 1 + \cos\left[\Delta\phi_i - \left(\Delta\varsigma_i - \Delta\varsigma_{i-1}\right) + \left(\Delta\xi_i - \Delta\xi_{i-1}\right)\right] \tag{69}$$
$$= 1 + \cos\left(\Delta\phi_i - \widehat{\Delta\phi_i} - \pi/2 - 2\,n_i\,\pi\right) = 1 + \sin\left(\Delta\phi_i - \widehat{\Delta\phi_i}\right)$$
$$= 1 + \left(\Delta\phi_i - \widehat{\Delta\phi_i}\right) - \left(\Delta\phi_i - \widehat{\Delta\phi_i}\right)^3/6 + \cdots$$

Taking the difference between W_i and W_{i-1} cancels the "1", yielding

$$W_i - W_{i-1} = \left(\Delta\phi_i - \widehat{\Delta\phi_i}\right) + \left(\Delta\phi_{i-1} - \widehat{\Delta\phi_{i-1}}\right) - \left(\Delta\phi_i - \widehat{\Delta\phi_i}\right)^3/6 - \left(\Delta\phi_{i-1} - \widehat{\Delta\phi_{i-1}}\right)^3/6 + \cdots \tag{70}$$

which permits $\Delta\phi_i$ determination without "1" scale factor accuracy dependence:

$$\Delta\phi_i = \widehat{\Delta\phi_i} - \Delta\phi_{i-1} + \widehat{\Delta\phi_{i-1}} + \left(W_i - W_{i-1}\right) + \left(\Delta\phi_i - \widehat{\Delta\phi_i}\right)^3/6 + \left(\Delta\phi_{i-1} - \widehat{\Delta\phi_{i-1}}\right)^3/6 + \cdots \tag{71}$$

(Note in Fig. 4 that analog negative bias is applied to the photo detector output before sampling by the D/A converter. This generates a bias on the measured W_i and W_{i-1} signals in (71) which cancels when calculating $W_i - W_{i-1}$, including cancellation of error that may be present in the applied analog bias signal. This characteristic will be used subsequently to eliminate round-off error in closed-loop control operations.)

Finally, we assume that the $\Delta\phi$ increments will have very little change over the time interval for a photon to traverse the fiber coil so that $\Delta\phi_i \approx \Delta\phi_{i-1}$ and $\Delta\phi_{i-1} \approx \Delta\phi_{i-2}$. We can, therefore, set the $\widehat{\Delta\phi_i}$, $\widehat{\Delta\phi_{i-1}}$ estimates to

$$\widehat{\Delta\phi_i} = \Delta\phi_{i-1} \qquad \widehat{\Delta\phi_{i-1}} = \Delta\phi_{i-2} \tag{72}$$

Additionally, we assume that using $\widehat{\Delta\phi_i}$ from (72), the $\left(\Delta\phi_i - \widehat{\Delta\phi_i}\right)^3$ term in (71) will change very slowly from cycle to cycle so that

$$\left(\Delta\phi_i - \widehat{\Delta\phi_i}\right)^3 \approx \left(\Delta\phi_i - \Delta\phi_{i-1}\right)^3 \approx \left(\Delta\phi_{i-1} - \Delta\phi_{i-2}\right)^3 \tag{73}$$

With (72) and (73), Eqs. (69), (70), and (71) become

$$\begin{aligned} W_{i-1} &= 1 + \cos\left[\Delta\phi_{i-1} - \left(\Delta\varsigma_{i-1} - \Delta\varsigma_{i-2}\right) + \left(\Delta\xi_{i-1} - \Delta\xi_{i-2}\right)\right] \\ &= 1 + \cos\left(\Delta\phi_{i-1} - \Delta\phi_{i-2} + \pi/2 - 2\,n_{i-1}\,\pi\right) \\ W_i &= 1 + \cos\left[\Delta\phi_i - \left(\Delta\varsigma_i - \Delta\varsigma_{i-1}\right) + \left(\Delta\xi_i - \Delta\xi_{i-1}\right)\right] \\ &= 1 + \cos\left(\Delta\phi_i - \Delta\phi_{i-1} - \pi/2 - 2\,n_i\,\pi\right) \\ \Delta\phi_i &= \Delta\phi_{i-2} + \left(W_i - W_{i-1}\right) + \left(\Delta\phi_{i-1} - \Delta\phi_{i-2}\right)^3/3 \end{aligned} \tag{74}$$

The identical process would be used during the next cycle to calculate $\Delta\phi_{i+1}$ from W_{i+1} and W_i power measurements using W_i from (74), $\widehat{\Delta\phi_i}$ from the (72) control law, (73) for the cubic term approximation, and their W_{i+1}, $\widehat{\Delta\phi_{i+1}}$ equivalents at t_{i+1}:

$$\begin{aligned} W_i &= 1 + \cos\left[\Delta\phi_i - \left(\Delta\varsigma_i - \Delta\varsigma_{i-1}\right) + \left(\Delta\xi_i - \Delta\xi_{i-1}\right)\right] \\ &= 1 + \cos\left(\Delta\phi_i - \Delta\phi_{i-1} - \pi/2 - 2\,n_i\,\pi\right) \\ W_{i+1} &= 1 + \cos\left[\Delta\phi_{i+1} - \left(\Delta\varsigma_{i+1} - \Delta\varsigma_i\right) + \left(\Delta\xi_{i+1} - \Delta\xi_i\right)\right] \\ &= 1 + \cos\left(\Delta\phi_{i+1} - \Delta\phi_i + \pi/2 - 2\,n_{i+1}\,\pi\right) \\ \Delta\phi_{i+1} &= \Delta\phi_{i-1} - \left(W_{i+1} - W_i\right) + \left(\Delta\phi_i - \Delta\phi_{i-1}\right)^3/3 \end{aligned} \tag{75}$$

Note the difference in polarity for $(W_{i+1} - W_i)$ in (75) compared with $(W_i - W_{i-1})$ in (74). The variation is caused by the difference in $\pi/2$ term polarities in the (75) $W_i \to W_{i+1}$ sequence compared with the $W_{i-1} \to W_i$ sequence in (74). Thus, recursive computations for sequential $\Delta\phi$ determination must account for alternating signs on both the $\pi/2$ and $(W_i - W_{i-1})$, $(W_{i+1} - W_i)$ terms in (74) and (75).

It remains to define settings for the $\Delta\varsigma$ s and $\Delta\xi$ s that satisfy (74) (and its next cycle (75) equivalent):

$$\begin{aligned}(\Delta\varsigma_{i-1} - \Delta\varsigma_{i-2}) - (\Delta\xi_{i-1} - \Delta\xi_{i-2}) &= \Delta\phi_{i-2} - \pi/2 + 2\,n_{i-1}\,\pi \\ (\Delta\varsigma_i - \Delta\varsigma_{i-1}) - (\Delta\xi_i - \Delta\xi_{i-1}) &= \Delta\phi_{i-1} + \pi/2 + 2\,n_i\,\pi\end{aligned} \tag{76}$$

A potential solution for the $\Delta\varsigma$ s and $\Delta\xi$ s in (76) might be to assign the alternating $\pi/2$ operations to the $\Delta\xi$ s, with the remaining $\Delta\phi_{i-2} + 2\,n_{i-1}\,\pi$ and $\Delta\phi_{i-1} + 2\,n_i\,\pi$ control operations assigned to the $\Delta\varsigma$ s. Another solution might be to set the $\Delta\xi$ s to zero (i.e., equating $\Delta\xi_i - \Delta\xi_{i-1} = 0$ and $\Delta\xi_{i-1} - \Delta\xi_{i-2} = 0$), and assign all operations in (76) to the $\Delta\varsigma$ s. In effect, this would represent a single L/N crystal biasing approach, implemented in Fig. 4 by maintaining the $\Delta\xi$ crystal presence (for component symmetry), but setting the V_ξ voltage to zero. This would also allow a lower manufacturing cost option by eliminating the $\Delta\xi$ crystal entirely, i.e., an unsymmetrical single crystal approach. Appendix C discusses the single crystal approach in detail.

Another, but fully symmetric solution (and the one discussed for the remainder of this section), derives by first equating n_i to $n_{\varsigma_i} + n_{\xi_i}$, and n_{i-1} to $n_{\varsigma_{i-1}} + n_{\xi_{i-1}}$ where n_{ς_i}, n_{ξ_i}, $n_{\varsigma_{i-1}}$, $n_{\xi_{i-1}}$ are integers. Thus, (76) becomes

$$\begin{aligned}(\Delta\varsigma_{i-1} - \Delta\varsigma_{i-2}) - (\Delta\xi_{i-1} - \Delta\xi_{i-2}) &= \Delta\phi_{i-2} - \pi/2 + 2\left(n_{\varsigma_{i-1}} + n_{\xi_{i-1}}\right)\pi \\ (\Delta\varsigma_i - \Delta\varsigma_{i-1}) - (\Delta\xi_i - \Delta\xi_{i-1}) &= \Delta\phi_{i-1} + \pi/2 + 2\left(n_{\varsigma_i} + n_{\xi_i}\right)\pi\end{aligned} \tag{77}$$

Dividing (77) into symmetrical $\Delta\varsigma$ and $\Delta\xi$ portions obtains

$$\begin{aligned}(\Delta\varsigma_{i-1} - \Delta\varsigma_{i-2}) &= \Delta\phi_{i-2}/2 - \pi/4 + 2\,n_{\varsigma_{i-1}}\,\pi \\ (\Delta\xi_{i-1} - \Delta\xi_{i-2}) &= -\Delta\phi_{i-2}/2 + \pi/4 - 2\,n_{\xi_{i-1}}\,\pi \\ (\Delta\varsigma_i - \Delta\varsigma_{i-1}) &= \Delta\phi_{i-1}/2 + \pi/4 + 2\,n_{\varsigma_i}\,\pi \\ (\Delta\xi_i - \Delta\xi_{i-1}) &= -\Delta\phi_{i-1}/2 - \pi/4 - 2\,n_{\xi_i}\,\pi\end{aligned} \tag{78}$$

Note that (77) equals the difference between the $\Delta\varsigma$ and $\Delta\xi$ expressions in (78). The recursive equivalent for the $\Delta\varsigma$ s and $\Delta\xi$ s in (78) then becomes

$$\begin{aligned}
\Delta\varsigma_{i-1} &= \Delta\varsigma_{i-2} + \Delta\phi_{i-2}/2 - \pi/4 + 2\,n_{\varsigma i-1}\,\pi \\
\Delta\xi_{i-1} &= \Delta\xi_{i-2} - \Delta\phi_{i-2}/2 + \pi/4 - 2\,n_{\xi i-1}\,\pi \\
\Delta\varsigma_{i} &= \Delta\varsigma_{i-1} + \Delta\phi_{i-1}/2 + \pi/4 + 2\,n_{\varsigma i}\,\pi \\
\Delta\xi_{i} &= \Delta\xi_{i-1} - \Delta\phi_{i-1}/2 - \pi/4 - 2\,n_{\xi i}\,\pi
\end{aligned} \tag{79}$$

Eqs. (79) with the $\Delta\theta$ output from $\Delta\phi$ in (64) are the basis for the symmetric closed-loop FOG computations shown in Fig. 6. The W^*_{i-1} and W^*_i signals in Fig. 6 represent the A/D Converter outputs in Fig. 4 including the negative bias (that is eliminated by the $W^*_i - W^*_{i-1}$ subtraction process), i.e.,

$$\begin{aligned}
W^*_{i-1} &= W_{i-1} - W_{Bias} \qquad W^*_i = W_i - W_{Bias} \\
W^*_i - W^*_{i-1} &= W_i - W_{i-1}
\end{aligned}. \tag{80}$$

where W_{Bias} is the negative bias in Fig. 4 applied to the photo detector output. Then from (74) with (80),

$$\begin{aligned}
\Delta\phi_i &= \Delta\phi_{i-2} + (W_i - W_{i-1}) + (\Delta\phi_{i-1} - \Delta\phi_{i-2})^3/3 \\
&= \Delta\phi_{i-2} + (W^*_i - W^*_{i-1}) + (\Delta\phi_{i-1} - \Delta\phi_{i-2})^3/3
\end{aligned} \tag{81}$$

which is used in Fig. 6 with (B-8) from Appendix B when calculating $\Delta\theta$ for output.

The *Sgn* term in the $\Delta\varsigma_i$, $\Delta\xi_i$ computations of Fig. 6 accounts for alternating polarities in $\pi/4$ compared with next cycle equivalents in (79). The *Sgn* term is also used in the $\Delta\phi_i$ computation of Fig. 6 to account for alternating polarities in $(W_i - W_{i-1})$ compared with next cycle equivalents in (74) and (75). The $2\,n_\varsigma\,\pi$, $2\,n_\xi\,\pi$ terms in (79) are used to assure that $\Delta\varsigma$, $\Delta\xi$ values applied to the lithium-niobate (L/N) crystals in Fig. 4 remain positive (greater than $\Delta\beta_{OffSet}$) and within a specified range for proper operation. This is achieved by logic statements in Fig. 6 that apply successive plus or minus 2π changes to $\Delta\varsigma$, $\Delta\xi$ until they satisfy the specified criteria.

Saved From Past Cycle : $\Delta\phi_{i-1}, \Delta\phi_{i-2}, W^*_{i-1}, \Delta\varsigma_{i-1}, \Delta\xi_{i-1}, \delta\Delta\varsigma_{i-1}, \delta\Delta\xi_{i-1}, \delta\Delta\varsigma_{i-2}, \delta\Delta\xi_{i-2}, \Delta\Sigma_{i-1}, Sgn$

Start of Current Cycle

At t_i : Sample W^*_i

After t_i But Before t_{i+1} :

Read W^*_i From A/D Converter

Then Calculate :

$$Sgn = -Sgn$$

$$\Delta\varsigma_i = \Delta\varsigma_{i-1} + \Delta\phi_{i-1}/2 + Sgn\,\pi/4$$

$$DO\ Until\ \Delta\varsigma_i \le \Delta\beta_{OffSet} + 2\pi \quad IF\ \Delta\varsigma_i > \Delta\beta_{OffSet} + 2\pi\ \ Then\ \ \Delta\varsigma_i = \Delta\varsigma_i - 2\pi$$

$$DO\ Until\ \Delta\varsigma_i \ge \Delta\beta_{OffSet} \quad IF\ \Delta\varsigma_i < \Delta\beta_{OffSet}\ \ Then\ \ \Delta\varsigma_i = \Delta\varsigma_i + 2\pi$$

$$\Delta\xi_i = \Delta\xi_{i-1} - \Delta\phi_{i-1}/2 - Sgn\,\pi/4$$

$$DO\ Until\ \Delta\xi_i \le \Delta\beta_{OffSet} + 2\pi \quad IF\ \Delta\xi_i > \Delta\beta_{OffSet} + 2\pi\ \ Then\ \ \Delta\xi_i = \Delta\xi_i - 2\pi$$

$$DO\ Until\ \Delta\xi_i \ge \Delta\beta_{OffSet} \quad IF\ \Delta\xi_i < \Delta\beta_{OffSet}\ \ Then\ \ \Delta\xi_i = \Delta\xi_i + 2\pi$$

$$\widehat{\Delta\varsigma_i} = \mathrm{Round}\left(\Delta\varsigma_i\right) \qquad \widehat{\Delta\xi_i} = \mathrm{Round}\left(\Delta\xi_i\right)$$

$$\delta\Delta\varsigma_i = \widehat{\Delta\varsigma_i} - \Delta\varsigma_i \qquad \delta\Delta\xi_i = \widehat{\Delta\xi_i} - \Delta\xi_i$$

$$\Delta\phi_i = \Delta\phi_{i-2} + \left(\Delta\phi_{i-1} - \Delta\phi_{i-2}\right)^3/3 + Sgn\left(W^*_i - W^*_{i-1}\right) + \left(\delta\Delta\varsigma_i - \delta\Delta\varsigma_{i-2}\right) - \left(\delta\Delta\xi_i - \delta\Delta\xi_{i-2}\right)$$

$$\Delta\theta_i = \Delta\phi_i / k_{SF}$$

$$\Sigma_i = \Delta\Sigma_{i-1} + \Delta\theta_i$$

$$\widehat{\Delta\theta_i} = \mathrm{Round}\left(\Sigma_i\right)$$

$$\Delta\Sigma_i = \Sigma_i - \widehat{\Delta\theta_i}$$

Output: $\widehat{\Delta\theta_i}$ As Digital Word To User

Output: $\widehat{\Delta\varsigma_i}, \widehat{\Delta\xi_i}$ Through D/A Converter And Apply To L/N Crystals

Save For Next Cycle : $\Delta\phi_i, \Delta\phi_{i-1}, W^*_i, \Delta\varsigma_i, \Delta\xi_i, \delta\Delta\varsigma_i, \delta\Delta\xi_i, \delta\Delta\varsigma_{i-1}, \delta\Delta\xi_{i-1}, \Delta\Sigma_i, Sgn$

Repeat For Next Cycle

Fig. 6 – Dual Crystal Closed-Loop FOG Symmetrical Computation Flow

The D/A Round operations in Fig. 6 round the computed $\Delta\varsigma$, $\Delta\xi$ values to $\widehat{\Delta\varsigma}$, $\widehat{\Delta\xi}$ at the same bit level as the Fig. 4 D/A converters, thereby eliminating round-off error that would occur in the D/A conversion process if $\Delta\varsigma$, $\Delta\xi$ were applied as computed (with uncertain round-off error then imposed on the L/N crystals in the D/A conversion process). Having $\left(W_i^* - W_{i-1}^*\right)$ in Fig. 6 computed based on applying rounded $\widehat{\Delta\varsigma}$, $\widehat{\Delta\xi}$ to the crystals would create error in calculating $\Delta\phi_i$ and the resulting $\Delta\theta_i$ output. However, the $\widehat{\Delta\varsigma}$, $\widehat{\Delta\xi}$ error is known (calculated as $\delta\Delta\varsigma$ and $\delta\Delta\xi$ in Fig. 6), hence, eliminated in Fig. 6 by correcting the $\left(W_i^* - W_{i-1}^*\right)$ value used in the $\Delta\phi_i$ calculation. A derivation of the $\delta\Delta\varsigma$ and $\delta\Delta\xi$ correction process is provided in Appendix B.

Additional round-off error can be generated when digitally outputting $\Delta\theta_i$ due to limited word length in the D/D (Digital-to-Digital) conversion function. This error is eliminated using a D/D Round function in Fig. 6, by computing $\widehat{\Delta\theta}$ (a rounded version of $\Delta\theta$), for output at the D/D function word length. The $\widehat{\Delta\theta}$ output is designed in Fig. 6 to assure that the sum of transmitted rounded $\widehat{\Delta\theta}$s equals the sum of the correct $\Delta\theta$s by cyclically controlling their summed difference $\Delta\Sigma$ to remain small. The result is a bounded error on the sum (integral) of the $\widehat{\Delta\theta}$s that varies randomly with magnitude of the lowest bit level in $\widehat{\Delta\theta}$.

Lastly, we address the round-off error generated in Fig. 6 when reading the W_{i-1}^* and W_i^* measurements through the A/D Converter in Fig. 4. This error is minimized by setting the analog negative bias signal in Fig. 4 to correspond with the expected unity value of the normalized photo detector W_i power measurement under closed-loop control. The result is an A/D converter input signal that is nominally zero, being only offset by the uncertainty in the photo detector output, the error in the analog bias, and the small dynamic lag in closed loop control operations. This enables scaling of the A/D converter so that the magnitude of the least significant bit (the effective round-off error) becomes negligible in the Fig. 6 calculations.

CONCLUSIONS

Optical gyros generate oppositely directed monochromatic light waves travelling in a closed-circuit waveguide to measure angular rotation relative to non-rotating inertial space. Based on classical Galilean/Newtonian kinematics and Relativity theory (under normal operating conditions), the wavelength of light waves in the waveguide will change due to angular rotation, increasing for waves travelling with rotation, decreasing for waves travelling against rotation. Due to Relativity theory, the velocity of the waves will remain constant (at the speed of light) relative to any point on the waveguide. As a result, relative to the readout device in the waveguide, the frequency will decrease for waves travelling with rotation, and increase for waves travelling against rotation. Additionally, relative to any point on the waveguide during rotation, the time increment for a wave to traverse a given distance increment will be the same, independent of its motion relative to the rotation direction. A corollary is that relative to the

waveguide, the time interval for a wave to traverse a given distance will be the same for waves travelling in either direction.

Ring laser gyros (RLGs) and fiber optic gyros (FOGs) are integrating angular change sensing inertial instruments, both measuring increments of gyro angular rotation relative to non-rotating inertial space. The analytics describing RLG and FOG operations emanate from the same fundamental equation. RLGs and FOGs differ analytically in the method used to extract incremental angular data measurements for output. Application of the fundamental equation for each depends on the total travel time for a light wave to traverse the waveguide.

Due to the RLG He-Ne stimulated-emission process, a light wave in an RLG will continue to traverse the waveguide from lasing ignition. The result is a pair of continuous counter-travelling light waves that combine at the readout, generating an optical interference pattern across the readout zone. The interference pattern moves across readout photo detectors at a rate proportional to the frequency difference between the counter-travelling light waves. The frequency difference is proportional to angular rate. The RLG output measures the occurrence of each interference pattern traversal, each representing a known increment of angular rotation relative to non-rotating inertial space.

In contrast, each light wave in a FOG only traverses the waveguide once from the time it leaves the FOG photo diode light source until it arrives at the readout photo detector. In a FOG, rotation generates a phase difference at the readout between the counter-travelling light waves. The phase difference is proportional to the increment of angular rotation during the time for a wave to traverse the waveguide. When the counter-travelling waves combine at the readout, the phase difference generates a change in the combined wave optical power illuminating the photo detector. Suitable closed-loop electronics convert photo detector optical power measurements into angular increments for output, while generating commands to lithium-niobate biasing crystal inserts in the gyro wave path for closed-loop control.

APPENDIX A

DERIVATION OF EQ. (3) BASED ON RELATIVITY THEORY

The equivalent to (3) based on Relativity theory [5 Eq. (12-5); 6 Eq. (10.31)-(10.32)] is in its equivalent point-to-point differential form [4 Eq. (35)]:

$$d\underline{x}_{p/i} = d\underline{x}_{p/a} - \underline{v}_{i/a}\, dt_a + \left(\frac{1}{\sqrt{1 - v_{ai}^2 / c^2}} - 1 \right) \left(d\underline{x}_{p/a} \cdot \underline{v}_{i/a}\, \underline{v}_{i/a} / v_{ai}^2 - \underline{v}_{i/a}\, dt_a \right) \qquad \text{(A-1)}$$

where $\underline{v}_{i/a}$ is the instantaneous velocity of point *i* as observed at point *a*, v_{ai} is the magnitude of $\underline{v}_{i/a}$, dt_a is the differential time interval for a differential change $d\underline{x}_{p/a}$ in the position location of a point *p* that would be measured at point *a*, and $d\underline{x}_{p/i}$ is the differential change in the point

p location that be measured at point *i* during dt_a. The peculiar $\sqrt{1-v_{ai}^2/c^2}$ term in (A-1) is a unique contribution from Relativity theory [4; 7 Appendix A] that assures that if point *p* is travelling at the speed of light *c*, the magnitude of *p* velocity relative to observation points *a* or *i* will be the same *c* constant:

$$\begin{aligned} \left|d\underline{x}_{p/a}/dt_a\right| &= \sqrt{\left(d\underline{x}_{p/a}/dt_{p_a}\right).\left(d\underline{x}_{p/a}/dt_a\right)} \\ &= \left|d\underline{x}_{p/i}/dt_i\right| = \sqrt{\left(d\underline{x}_{p/i}/dt_i\right).\left(d\underline{x}_{p/i}/dt_i\right)} = c \end{aligned} \qquad \text{(A-2)}$$

where dt_i is the time interval for the $d\underline{x}_{p/i}$ differential motion that would be measured on a clock located at point *i*.

Eq. (A-1) is also based on $\underline{v}_{a/i}$ (the velocity of point *a* observed at point *i*) being of equal magnitude but oppositely directed from $\underline{v}_{i/a}$ (the velocity of point *i* observed at point *)*, a fundamental premise of both classical Newtonian kinematics and Relativity theory [3 pp 236-238; 6 pp 30]:

$$\underline{v}_{i/a} \equiv \frac{d\underline{x}_{i/a}}{dt_a} \qquad \underline{v}_{a/i} \equiv \frac{d\underline{x}_{a/i}}{dt_i} \qquad \underline{v}_{a/i} = -\underline{v}_{i/a} \qquad v_{ai} \equiv \left|\underline{v}_{i/a}\right| = \left|\underline{v}_{a/i}\right| \qquad \text{(A-3)}$$

For the commonly encountered situations when $v_{ai} \ll c$, the $\sqrt{1-v_{ai}^2/c^2}$ Relativity coefficient in (A-1) approximates as unity and (A-1) simplifies to

$$d\underline{x}_{p/i} = d\underline{x}_{p/a} - \underline{v}_{i/a}\, dt_a \qquad \text{(A-4)}$$

Substituting $\underline{v}_{i/a}\, dt_a = d\underline{x}_{i/a}$ from (A-3) into (A-4) obtains with rearrangement

$$d\underline{x}_{p/a} = d\underline{x}_{p/i} + d\underline{x}_{i/a} \qquad \text{(A-5)}$$

With the differentials in (A-5) approximated as small finite Δ changes, (A-5) becomes (3) in the main text derived using classical Galilean/Newtonian kinematic theory:

$$\Delta\underline{x}_{p/a} = \Delta\underline{x}_{p/i} + \Delta\underline{x}_{i/a} \qquad \text{(A-6)}$$

APPENDIX B

DERIVING ROUND-OFF ERROR CORRECTIONS TO FOG LITHIUM-NIOBATE CRYSTAL COMMAND VOLTAGES

This appendix derives the $\Delta\phi_i$ equation in Fig. 6 used to correct the error generated using rounded $\widehat{\Delta\varsigma}$, $\widehat{\Delta\xi}$ data for biasing the L/N crystals in Fig. 4. The derivation begins with definitions for $\widehat{\Delta\varsigma}$, $\widehat{\Delta\xi}$ in terms of non-rounded $\Delta\varsigma$, $\Delta\xi$ and the $\delta\Delta\varsigma$, $\delta\Delta\xi$ round-off errors in Fig. 6:

$$\begin{aligned}
\widehat{\Delta\varsigma_{i-1}} &= \Delta\varsigma_{i-1} + \delta\Delta\varsigma_{i-1} \qquad \widehat{\Delta\varsigma_{i-2}} = \Delta\varsigma_{i-2} + \delta\Delta\varsigma_{i-2} \\
\widehat{\Delta\xi_{i-1}} &= \Delta\xi_{i-1} + \delta\Delta\xi_{i-1} \qquad \widehat{\Delta\xi_{i-2}} = \Delta\xi_{i-2} + \delta\Delta\xi_{i-2} \\
\widehat{\Delta\varsigma_{i}} &= \Delta\varsigma_{i} + \delta\Delta\varsigma_{i} \qquad \widehat{\Delta\varsigma_{i-1}} = \Delta\varsigma_{i-1} + \delta\Delta\varsigma_{i-1} \\
\widehat{\Delta\xi_{i}} &= \Delta\xi_{i} + \delta\Delta\xi_{i} \qquad \widehat{\Delta\xi_{i-1}} = \Delta\xi_{i-1} + \delta\Delta\xi_{i-1}
\end{aligned} \tag{B-1}$$

Use of rounded L/N input produces combined power values W having the same form as (65) – (66), but with $\Delta\varsigma$, $\Delta\xi$ replaced by $\widehat{\Delta\varsigma}$, $\widehat{\Delta\xi}$:

$$\begin{aligned}
W_{i-1} &= 1 + \cos\left[\Delta\phi_{i-1} - \left(\widehat{\Delta\varsigma_{i-1}} - \widehat{\Delta\varsigma_{i-2}}\right) + \left(\widehat{\Delta\xi_{i-1}} - \widehat{\Delta\xi_{i-2}}\right)\right] \\
W_{i} &= 1 + \cos\left[\Delta\phi_{i} - \left(\widehat{\Delta\varsigma_{i}} - \widehat{\Delta\varsigma_{i-1}}\right) + \left(\widehat{\Delta\xi_{i}} - \widehat{\Delta\xi_{i-1}}\right)\right]
\end{aligned} \tag{B-2}$$

Substituting (B-1) into (B-2) obtains

$$\begin{aligned}
W_{i-1} &= 1 + \cos\left[\Delta\phi_{i-1} - \left(\widehat{\Delta\varsigma_{i-1}} - \widehat{\Delta\varsigma_{i-2}}\right) + \left(\widehat{\Delta\xi_{i-1}} - \widehat{\Delta\xi_{i-2}}\right)\right] \\
&= 1 + \cos\left\{\begin{array}{l}\Delta\phi_{i-1} - \left[\left(\Delta\varsigma_{i-1} + \delta\Delta\varsigma_{i-1}\right) - \left(\Delta\varsigma_{i-2} + \delta\Delta\varsigma_{i-2}\right)\right] \\ \quad + \left[\left(\Delta\xi_{i-1} + \delta\Delta\xi_{i-1}\right) - \left(\Delta\xi_{i-2} + \delta\Delta\xi_{i-2}\right)\right]\end{array}\right\} \\
&= 1 + \cos\left[\begin{array}{c}\Delta\phi_{i-1} - \left(\Delta\varsigma_{i-1} - \Delta\varsigma_{i-2}\right) + \left(\Delta\xi_{i-1} - \Delta\xi_{i-2}\right) \\ -\left(\delta\Delta\varsigma_{i-1} - \delta\Delta\varsigma_{i-2}\right) + \left(\delta\Delta\xi_{i-1} - \delta\Delta\xi_{i-2}\right)\end{array}\right]
\end{aligned} \tag{B-3}$$

$$\begin{aligned}
W_{i} &= 1 + \cos\left[\Delta\phi_{i} - \left(\widehat{\Delta\varsigma_{i}} - \widehat{\Delta\varsigma_{i-1}}\right) + \left(\widehat{\Delta\xi_{i}} - \widehat{\Delta\xi_{i-1}}\right)\right] \\
&= 1 + \cos\left\{\Delta\phi_{i} - \left[\left(\Delta\varsigma_{i} + \delta\Delta\varsigma_{i}\right) - \left(\Delta\varsigma_{i-1} + \delta\Delta\varsigma_{i-1}\right)\right] + \left[\left(\Delta\xi_{i} + \delta\Delta\xi_{i}\right) - \left(\Delta\xi_{i-1} + \delta\Delta\xi_{i-1}\right)\right]\right\} \\
&= 1 + \cos\left[\Delta\phi_{i} - \left(\Delta\varsigma_{i} - \Delta\varsigma_{i-1}\right) + \left(\Delta\xi_{i} - \Delta\xi_{i-1}\right) - \left(\delta\Delta\varsigma_{i} - \delta\Delta\varsigma_{i-1}\right) + \left(\delta\Delta\xi_{i} - \delta\Delta\xi_{i-1}\right)\right]
\end{aligned}$$

The unrounded $\left(\Delta\varsigma_{i-1}-\Delta\varsigma_{i-2}\right)$, $\left(\Delta\xi_{i-1}-\Delta\xi_{i-2}\right)$, $\left(\Delta\varsigma_{i}-\Delta\varsigma_{i-1}\right)$, $\left(\Delta\xi_{i}-\Delta\xi_{i-1}\right)$ terms in (B-3) are from (78):

$$\begin{aligned}
\left(\Delta\varsigma_{i-1}-\Delta\varsigma_{i-2}\right) &= \Delta\phi_{i-2}/2-\pi/4+2\,n_{\varsigma_{i-1}}\pi \\
\left(\Delta\xi_{i-1}-\Delta\xi_{i-2}\right) &= -\Delta\phi_{i-2}/2+\pi/4-2\,n_{\xi_{i-1}}\pi \\
\left(\Delta\varsigma_{i}-\Delta\varsigma_{i-1}\right) &= \Delta\phi_{i-1}/2+\pi/4+2\,n_{\varsigma_{i}}\pi \\
\left(\Delta\xi_{i}-\Delta\xi_{i-1}\right) &= -\Delta\phi_{i-1}/2-\pi/4-2\,n_{\xi_{i}}\pi
\end{aligned} \qquad \text{(B-4)}$$

Substituting (B-4) into (B-3) then gives

$$\begin{aligned}
W_{i-1} &= 1+\cos\begin{bmatrix}\Delta\phi_{i-1}-\Delta\phi_{i-2}+\pi/2-2\left(n_{\varsigma_{i-1}}+n_{\xi_{i-1}}\right)\pi \\ -\left(\delta\Delta\varsigma_{i-1}-\delta\Delta\varsigma_{i-2}\right)+\left(\delta\Delta\xi_{i-1}-\delta\Delta\xi_{i-2}\right)\end{bmatrix} \\
&= 1-\sin\left[\Delta\phi_{i-1}-\Delta\phi_{i-2}-\left(\delta\Delta\varsigma_{i-1}-\delta\Delta\varsigma_{i-2}\right)+\left(\delta\Delta\xi_{i-1}-\delta\Delta\xi_{i-2}\right)\right] \\
&\approx 1-\left[\Delta\phi_{i-1}-\Delta\phi_{i-2}-\left(\delta\Delta\varsigma_{i-1}-\delta\Delta\varsigma_{i-2}\right)+\left(\delta\Delta\xi_{i-1}-\delta\Delta\xi_{i-2}\right)\right] \\
&= 1-\Delta\phi_{i-1}+\Delta\phi_{i-2}+\left(\delta\Delta\varsigma_{i-1}-\delta\Delta\varsigma_{i-2}\right)-\left(\delta\Delta\xi_{i-1}-\delta\Delta\xi_{i-2}\right)
\end{aligned} \qquad \text{(B-5)}$$

$$\begin{aligned}
W_i &= 1+\cos\left[\Delta\phi_i-\Delta\phi_{i-1}-\pi/2-2\left(\,n_{\varsigma_i}+n_{\xi_i}\right)\pi-\left(\delta\Delta\varsigma_i-\delta\Delta\varsigma_{i-1}\right)+\left(\delta\Delta\xi_i-\delta\Delta\xi_{i-1}\right)\right] \\
&= 1+\sin\left[\Delta\phi_i-\Delta\phi_{i-1}-\left(\delta\Delta\varsigma_i-\delta\Delta\varsigma_{i-1}\right)+\left(\delta\Delta\xi_i-\delta\Delta\xi_{i-1}\right)\right] \\
&\approx 1+\Delta\phi_i-\Delta\phi_{i-1}-\left(\delta\Delta\varsigma_i-\delta\Delta\varsigma_{i-1}\right)+\left(\delta\Delta\xi_i-\delta\Delta\xi_{i-1}\right)
\end{aligned}$$

Subtracting W_{i-1} from W_i in (B-5) obtains

$$\begin{aligned}
W_i-W_{i-1} &= \Delta\phi_i-\Delta\phi_{i-1}-\left(\delta\Delta\varsigma_i-\delta\Delta\varsigma_{i-1}\right)+\left(\delta\Delta\xi_i-\delta\Delta\xi_{i-1}\right) \\
&+\Delta\phi_{i-1}-\Delta\phi_{i-2}-\left(\delta\Delta\varsigma_{i-1}-\delta\Delta\varsigma_{i-2}\right)+\left(\delta\Delta\xi_{i-1}-\delta\Delta\xi_{i-2}\right) \\
&= \Delta\phi_i-\Delta\phi_{i-2}-\left(\delta\Delta\varsigma_i-\delta\Delta\varsigma_{i-2}\right)+\left(\delta\Delta\xi_i-\delta\Delta\xi_{i-2}\right)
\end{aligned} \qquad \text{(B-6)}$$

from which

$$\Delta\phi_i=\Delta\phi_{i-2}+\left(W_i-W_{i-1}\right)+\left(\delta\Delta\varsigma_i-\delta\Delta\varsigma_{i-2}\right)-\left(\delta\Delta\xi_i-\delta\Delta\xi_{i-2}\right) \qquad \text{(B-7)}$$

The identical procedure for the next cycle finds

$$\widehat{\Delta\varsigma_{i+1}} = \Delta\varsigma_{i+1} + \delta\Delta\varsigma_{i+1} \qquad \widehat{\Delta\varsigma_i} = \Delta\varsigma_i + \delta\Delta\varsigma_i$$
$$\widehat{\Delta\xi_{i+1}} = \Delta\xi_{i+1} + \delta\Delta\xi_{i+1} \qquad \widehat{\Delta\xi_i} = \Delta\xi_i + \delta\Delta\xi_i$$

$$W_{i+1} = 1 + \cos\left[\Delta\phi_{i+1} - \left(\widehat{\Delta\varsigma_{i+1}} - \widehat{\Delta\varsigma_i}\right) + \left(\widehat{\Delta\xi_{i+1}} - \widehat{\Delta\xi_i}\right)\right]$$
$$= 1 + \cos\left[\Delta\phi_{i+1} - \left(\Delta\varsigma_{i+1} - \Delta\varsigma_i\right) + \left(\Delta\xi_{i+1} - \Delta\xi_i\right) - \left(\delta\Delta\varsigma_{i+1} - \delta\Delta\varsigma_i\right) + \left(\delta\Delta\xi_{i+1} - \delta\Delta\xi_i\right)\right] \tag{B-8}$$
$$\left(\Delta\varsigma_{i+1} - \Delta\varsigma_i\right) = \Delta\phi_i / 2 - \pi / 4 + 2\, n_{\varsigma_{i+1}}\pi$$
$$\left(\Delta\xi_{i+1} - \Delta\xi_i\right) = -\Delta\phi_i / 2 + \pi / 4 - 2\, n_{\xi_{i+1}}\pi$$

$$W_{i+1} = 1 + \cos\left[\Delta\phi_{i+1} - \Delta\phi_i + \pi/2 - 2\left(n_{\varsigma_{i+1}} + n_{\xi_{i+1}}\right)\pi - \left(\delta\Delta\varsigma_{i+1} - \delta\Delta\varsigma_i\right) + \left(\delta\Delta\xi_{i+1} - \delta\Delta\xi_i\right)\right]$$
$$= 1 - \sin\left[\Delta\phi_{i+1} - \Delta\phi_i - \left(\delta\Delta\varsigma_{i+1} - \delta\Delta\varsigma_i\right) + \left(\delta\Delta\xi_{i+1} - \delta\Delta\xi_i\right)\right]$$
$$\approx 1 - \Delta\phi_{i+1} + \Delta\phi_i + \left(\delta\Delta\varsigma_{i+1} - \delta\Delta\varsigma_i\right) - \left(\delta\Delta\xi_{i+1} - \delta\Delta\xi_i\right)$$

Subtracting W_i in (B-5) from W_{i+1} in (B-8) obtains

$$W_{i+1} - W_i = -\left(\Delta\phi_{i+1} - \Delta\phi_i\right) + \left(\delta\Delta\varsigma_{i+1} - \delta\Delta\varsigma_i\right) - \left(\delta\Delta\xi_{i+1} - \delta\Delta\xi_i\right)$$
$$-\left[\Delta\phi_i - \Delta\phi_{i-1} - \left(\delta\Delta\varsigma_i - \delta\Delta\varsigma_{i-1}\right) + \left(\delta\Delta\xi_i - \delta\Delta\xi_{i-1}\right)\right] \tag{B-9}$$
$$= -\Delta\phi_{i+1} + \Delta\phi_{i-1} + \left(\delta\Delta\varsigma_{i+1} - \delta\Delta\varsigma_{i-1}\right) - \left(\delta\Delta\xi_{i+1} - \delta\Delta\xi_{i-1}\right)$$

from which,

$$\Delta\phi_{i+1} = \Delta\phi_{i-1} - \left(W_{i+1} - W_i\right) + \left(\delta\Delta\varsigma_{i+1} - \delta\Delta\varsigma_{i-1}\right) - \left(\delta\Delta\xi_{i+1} - \delta\Delta\xi_{i-1}\right) \tag{B-10}$$

Thus, for two successive cycles, (B-7) and (B-10) show that

$$\Delta\phi_i = \Delta\phi_{i-2} + \left(W_i - W_{i-1}\right) + \left(\delta\Delta\varsigma_i - \delta\Delta\varsigma_{i-2}\right) - \left(\delta\Delta\xi_i - \delta\Delta\xi_{i-2}\right)$$
$$\Delta\phi_{i+1} = \Delta\phi_{i-1} - \left(W_{i+1} - W_i\right) + \left(\delta\Delta\varsigma_{i+1} - \delta\Delta\varsigma_{i-1}\right) - \left(\delta\Delta\xi_{i+1} - \delta\Delta\xi_{i-1}\right) \tag{B-11}$$

The (B-11) expressions are identical except for the difference in polarity for the W power difference term in $\Delta\phi_{i+1}$ compared with its equivalent in $\Delta\phi_i$. A common formula for both can be defined as

$$\Delta\phi_i = \Delta\phi_{i-2} + Sgn\left(W_i - W_{i-1}\right) + \left(\delta\Delta\varsigma_i - \delta\Delta\varsigma_{i-2}\right) - \left(\delta\Delta\xi_i - \delta\Delta\xi_{i-2}\right) \tag{B-12}$$

where *Sgn* is unity in magnitude and alternating in polarity from *i* cycle to *i* cycle. Eq. (B-12) is what is shown with (81) in Fig. 6, with from (B-1):

$$\begin{aligned} \delta\Delta\varsigma_{i-1} &= \widehat{\Delta\varsigma_{i-1}} - \Delta\varsigma_{i-1} \qquad \delta\Delta\varsigma_{i-2} = \widehat{\Delta\varsigma_{i-2}} - \Delta\varsigma_{i-2} \\ \delta\Delta\xi_{i-1} &= \widehat{\Delta\xi_{i-1}} - \Delta\xi_{i-1} \qquad \delta\Delta\xi_{i-2} = \widehat{\Delta\xi_{i-2}} - \Delta\xi_{i-2} \end{aligned} \tag{B-13}$$

APPENDIX C

SINGLE CRYSTAL CLOSED LOOP CONTROL

A single lithium-niobate crystal biasing approach can be used for closed-loop FOG operations by setting the $\Delta\xi$ s in Fig. 4 to zero so that the recursive form of (77) becomes

$$\begin{aligned} \Delta\varsigma_{i-1} &= \Delta\varsigma_{i-2} + \Delta\phi_{i-2} - \pi/2 + 2\, n_{\varsigma_{i-1}}\pi \\ \Delta\varsigma_{i} &= \Delta\varsigma_{i-1} + \Delta\phi_{i-1} + \pi/2 + 2\, n_{\varsigma_{i}}\pi \end{aligned} \tag{C-1}$$

Eqs. (C-1) with (81) for $\Delta\phi_i$ and $\Delta\theta$ output from $\Delta\phi$ in (64), are the basis for the single crystal closed-loop FOG computation operations shown in Fig. 7.

In Fig. 7, the W^*_{i-1} and W^*_i signals represent the A/D Converter output in Fig. 4 including the negative bias applied to the photo detector output. The *Sgn* term in Fig. 7 accounts for $\pi/2$ and $(W_i - W_{i-1})$ alternating polarities in (74) compared with their next cycle equivalents in (75). The $2\, n_\varsigma \pi$ term in (C-1) is used to assure that the $\Delta\varsigma$ value applied to the lithium-niobate (L/N) cell in Fig. 4 remains positive (greater than $\Delta\beta_{OffSet}$) and within a specified range for proper operation. This is achieved by logic statements in Fig. 7 that apply successive plus or minus 2π changes to $\Delta\varsigma$ until it satisfies the specified criteria.

The D/A Round operations in Fig. 7 round the computed $\Delta\varsigma$ values to $\widehat{\Delta\varsigma}$ for output at the same bit level as the Fig. 4 $\Delta\varsigma$ D/A converter, thereby eliminating round-off error that would occur in the D/A conversion process if $\Delta\varsigma$ were applied as computed (with uncertain round-off error then imposed on the L/N crystals in the D/A conversion process). Having $W^*_i - W^*_{i-1}$ in Fig. 7 computed based on applying rounded $\widehat{\Delta\varsigma}$ to the crystal would create error in calculating $\Delta\phi_i$ and the resulting $\Delta\theta_i$ output. However, the $\widehat{\Delta\varsigma}$ error is known (calculated as $\delta\Delta\varsigma$ in Fig. 7), thus, eliminated in Fig. 7 by correcting the $\left(W^*_i - W^*_{i-1}\right)$ value used in the $\Delta\phi_i$ calculation. A derivation of the $\delta\Delta\varsigma$ correction process is provided in Appendix B.

Saved From Past Cycle : $\Delta\phi_{i-1}, \Delta\phi_{i-2}, W^*_{i-1}, \Delta\varsigma_{i-1}, \delta\Delta\varsigma_{i-1}, \delta\Delta\varsigma_{i-2}, \Delta\Sigma_{i-1}, Sgn$

Start of Current Cycle

At t_i : Sample W^*_i

After t_i But Before t_{i+1} :

Read W^*_i From A/D Converter

Then Calculate :

$$Sgn = -Sgn$$

$$\Delta\varsigma_i = \Delta\varsigma_{i-1} + \Delta\phi_{i-1} + Sgn\ \pi / 2$$

$$DO\ Until\ \Delta\varsigma_i \le \Delta\beta_{OffSet} + 2\pi \quad IF\ \Delta\varsigma_i > \Delta\beta_{OffSet} + 2\pi\ \ Then\ \ \Delta\varsigma_i = \Delta\varsigma_i - 2\pi$$

$$DO\ Until\ \Delta\varsigma_i \ge \Delta\beta_{OffSet} \quad IF\ \Delta\varsigma_i < \Delta\beta_{OffSet}\ \ Then\ \ \Delta\varsigma_i = \Delta\varsigma_i + 2\pi$$

$$\widehat{\Delta\varsigma_i} = \text{Round}\left(\Delta\varsigma_i\right)$$

$$\delta\Delta\varsigma_i = \widehat{\Delta\varsigma_i} - \Delta\varsigma_i$$

$$\Delta\phi_i = \Delta\phi_{i-2} + \left(\Delta\phi_{i-1} - \Delta\phi_{i-2}\right)^3 / 3 + Sgn\left(W^*_i - W^*_{i-1}\right) + \left(\delta\Delta\varsigma_i - \delta\Delta\varsigma_{i-2}\right)$$

$$\Delta\theta_i = \Delta\phi_i / k_{SF}$$

$$\Sigma_i = \Delta\Sigma_{i-1} + \Delta\theta_i$$

$$\widehat{\Delta\theta_i} = \text{Round}\left(\Sigma_i\right)$$

$$\Delta\Sigma_i = \Sigma_i - \widehat{\Delta\theta_i}$$

Output: $\widehat{\Delta\theta_i}$ As Digital Word To User

Output: $\widehat{\Delta\varsigma_i}$ Through D/A Converter And Apply To L/N Crystal

Save For Next Cycle : $\Delta\phi_i, \Delta\phi_{i-1}, W^*_i, \Delta\varsigma_i, \delta\Delta\varsigma_i, \delta\Delta\varsigma_{i-1}, \Delta\Sigma_i, Sgn$

Repeat For Next Cycle

Fig. 7 – Single Crystal Closed-Loop FOG Computation Flow

Additional round-off error can be generated when digitally outputting $\Delta\theta_i$ due to limited word length in the D/D (Digital-to-Digital) conversion function. This error is eliminated using a

D/D Round function in Fig. 7, by generating $\widehat{\Delta\theta}$ (a rounded version of $\Delta\theta$), for output at the D/D function word length. The $\widehat{\Delta\theta}$ output is designed in Fig. 7 to assure that the sum of transmitted rounded $\widehat{\Delta\theta}$s equals the sum of the correct $\Delta\theta$s by cyclically controlling their summed difference $\Delta\Sigma$ to remain small. The result is a bounded error on the sum (integral) of the $\widehat{\Delta\theta}$s that varies randomly at the magnitude of the lowest bit level in $\widehat{\Delta\theta}$.

Finally, we address the round-off error generated in Fig. 7 when reading the W_{i-1}^* and W_i^* measurements through the A/D Converter in Fig. 4. This error is minimized by setting the analog negative bias signal in Fig. 4 to correspond to the expected unity value of the normalized photo detector W_i power measurement under closed-loop control. The result is an A/D converter input signal that is nominally zero, being only offset by the uncertainty in the photo detector output, the error in the analog bias, and the small dynamic lag in closed loop control operations. This enables scaling of the A/D converter so that the magnitude of the least significant bit (the effective round-off error) becomes negligible in the Fig. 7 calculations.

REFERENCES

[1] Savage, P. G., "Analytically Deriving How Ring Laser And Fiber Optic Gyros Measure Angular Rotation", SAI WBN-14023, Nov 1, 2018 (Updated July 21, 2019). This is the original article now replaced with this 14024 updated version. The 14023 article has been removed from the www.strapdownassociates.com free-access website.

[2] Einstein, A., *Relativity, The Special and the General Theory*, 1961, The Estate of Albert Einstein.

[3] Born, Max, *Einstein's Theory of Relativity*, Dover Publications, Inc., New York.

[4] Savage, P. G., "Differential Kinematics Of Point-To-Point Relativity", SAI WBN-14021**,** March 11, 2018, free access available at www.strapdownassociates.com.

[5] Halfman, Robert L., *Dynamics: Systems, Variational Methods, Relativity, Volume II*, Addison-Wesley, 1962.

[6] Fock, V., *Theory of Space, Time, and Gravitation, Second Revised Edition*, New York: Pergamon Press, 1964

[7] Savage, P. G., "Differential Point-To-Point Relativity In Rotating Coordinates", SAI WBN-14022, May 28, 2018, free access available at www.strapdownassociates.com.

[8] Savage, P. G., *Strapdown Analytics, Edition II*, Strapdown Associates, Inc., 2007

[9] Savage, P. G., “Introduction To The Kinematics Of Point-To-Point Relativity”, WBN-14015, Strapdown Associates, Inc., April 17, 2016 (Updated January 29, 2018), free access available at www.strapdownassociates.com.

[10] Burington, R. S., *Handbook Of Mathematical Tables And Formulas*, R. S. Burington, 1933 – 1948, Handbook Publishers, Inc. Sandusky, OH

[11] Killpatrick, Joseph, "The Laser Gyro", IEEE Spectrum, Oct. 1967.

[12] Aronowitz, F., “Fundamentals of the Ring Laser Gyro”, Paper 3., *Optical Gyros And Their Applications*, NATO RTO-AG-339, May 1999.

[13] Lawrence, A., *Modern Inertial Technology*, Springer-Verlag 1993.

[14] Lefevre, C. L.., “Application Of The Sagnac Effect In The Interferometric Fiber-Optic Gyroscope”, Paper 7, *Optical Gyros And their Applications*, NATO RTO-AG-339, May 1999.

[15] Ezekiel, S. and Arditty, H.J., ed. *Fiber Optic Rotation Sensors and Related Technologies*, Springer-Verlag, Berlin/Heidelberg/New York, 1982.

[16] Savage, P.G., “Blazing Gyros – The Evolution of Strapdown Inertial Navigation Technology For Aircraft”, *AIAA Journal Of Guidance, Control, And Dynamics*, Vol. 36, No. 3, May - June, 2013, pp. 637-655, also posted for free-access as WBN-14009 at www.strapdownassociates.com.